










Little Ado about Everything: η CDM, a Cosmological Model with Fluctuation-driven Acceleration at Late Times

Andrea Lapi^{1,2,3,4} , Lumen Boco^{1,2} , Marcos M. Cueli^{1,2} , Balakrishna S. Haridasu^{1,2} , Tommaso Ronconi^{1,2} ,
Carlo Baccigalupi^{1,2,3,5} , and Luigi Danese^{1,2} 

¹ SISSA, Via Bonomea 265, I-34136 Trieste, Italy

² IFPU—Institute for Fundamental Physics of the Universe, Via Beirut 2, I-34014 Trieste, Italy

³ INFN-Sezione di Trieste, via Valerio 2, I-34127 Trieste, Italy

⁴ INAF/IRA, Istituto di Radioastronomia, Via Piero Gobetti 101, I-40129 Bologna, Italy

⁵ INAF, Osservatorio Astronomico di Trieste, Via G.B. Tiepolo 11, I-34131 Trieste, Italy

Received 2023 April 21; revised 2023 October 4; accepted 2023 October 8; published 2023 December 8

Abstract

We propose a model of the Universe (dubbed η CDM) featuring a controlled stochastic evolution of the cosmological quantities that is meant to render the effects of small deviations from homogeneity/isotropy on scales of $30\text{--}50 h^{-1}$ Mpc at late cosmic times associated with the emergence of the cosmic web. Specifically, we prescribe that the behavior of the matter/radiation energy densities in different patches of the Universe with such a size can be effectively described by a stochastic version of the mass–energy evolution equation. The latter includes, besides the usual dilution due to cosmic expansion, an appropriate noise term that statistically accounts for local fluctuations due to inhomogeneities, anisotropic stresses, and matter flows induced by complex gravitational processes. The evolution of the different patches as a function of cosmic time is rendered via the diverse realizations of the noise term; meanwhile, at any given cosmic time, sampling the ensemble of patches will create a nontrivial spatial distribution of the various cosmological quantities. Finally, the overall behavior of the Universe will be obtained by averaging over the patch ensemble. We assume a simple and physically reasonable parameterization of the noise term, gauging it against a wealth of cosmological data sets in the local and high-redshift Universe. We find that, with respect to standard Λ CDM, the ensemble-averaged cosmic dynamics in the η CDM model is substantially altered by the stochasticity in three main respects: (i) an accelerated expansion is enforced at late cosmic times without the need for any additional exotic component (e.g., dark energy), (ii) the spatial curvature can stay small even in a low-density Universe constituted solely by matter and radiation, (iii) matter can acquire an effective negative pressure at late times. The η CDM model is Hubble tension–free, meaning that the estimates of the Hubble constant from early- and late-time measurements do not show marked disagreement as in Λ CDM. We also provide specific predictions for the variance of the cosmological quantities among the different patches of the Universe at late cosmic times. Finally, the fate of the Universe in the η CDM model is investigated to show that the cosmic coincidence problem is relieved without invoking the anthropic principle.

Unified Astronomy Thesaurus concepts: [Cosmology \(343\)](#); [Cosmological models \(337\)](#); [Cosmological principle \(2363\)](#)

1. Introduction

The standard Λ CDM model of the Universe has proven to be extremely successful in reproducing to a high degree of accuracy many cosmological observations, most noticeably the cosmic microwave background (CMB) temperature and polarization spectra (e.g., Bennett et al. 2003; Planck Collaboration et al. 2013, 2020a), supernova (SN) Ia cosmography (e.g., Perlmutter et al. 1999; Scolnic et al. 2018; Brout et al. 2022), baryon acoustic oscillation (BAO) measurements (e.g., Eisenstein et al. 2005; Beutler et al. 2011; Zhao et al. 2022), cosmic shear galaxy surveys (e.g., Heymans et al. 2013; Amon et al. 2022; Secco et al. 2022), galaxy clusters (e.g., White et al. 1993; Allen et al. 2011; Mantz et al. 2022), and many others (e.g., see recent review by Turner 2022 and references therein; see also Efstathiou 2023). Despite these astonishing successes, the Λ CDM model maintains a

fundamentally empirical character, in that it postulates the existence of a mysterious dark energy component with exotic negative pressure that, at late cosmic times, dominates the energy budget and enforces an accelerated expansion of the Universe.

From an observational perspective, the evidence for dark energy remains mainly related to the interpretation of two occurrences: the accelerated expansion of the Universe at late cosmic times, as mainly indicated by Type Ia SN determinations of the magnitude–redshift diagram, and the nearly zero curvature (flat geometry) of a Universe with a low matter (baryons and dark matter) content, as mainly indicated by CMB and BAO data. From a theoretical perspective, the situation is even more dramatic; the value of the present dark energy density required to explain the aforementioned observations is far below the Planck or any natural scale in particle physics. Nonetheless, it is of the same order of magnitude with respect to the matter density, rather than extremely smaller or fatally larger, thus allowing its observability in this very precise moment of cosmic history (e.g., Zel’dovich 1968; Weinberg 1989). Furthermore, in recent years, some discrepancies with

the Λ CDM paradigm started to emerge with various degrees of significance, among them the (in)famous Hubble tension that concerns the disagreement between late-time measurements of the Hubble constant with respect to the Λ CDM predictions from the CMB (e.g., Efstathiou 2020; Riess et al. 2022; see also Di Valentino et al. 2021) and the S_8 tension that concerns a deficit in the weak lensing amplitude measured by cosmic shear galaxy surveys with respect to the CMB expectations (e.g., Asgari et al. 2021; Secco et al. 2022; see also Amon & Efstathiou 2022).

In this complex landscape, a number of alternative cosmological models have been designed with the aim to interpret the cosmic acceleration without invoking a dark energy component. For example, one may consider modified gravity theories that introduce additional degrees of freedom in the gravitational and/or matter action (see reviews by Clifton et al. 2012; Nojiri et al. 2017; Saridakis et al. 2021; see also Planck Collaboration et al. 2016), one may phenomenologically modify the Friedmann equation by additional terms that depend on the matter density in a nonlinear way like in the Cardassian scenarios (see Freese & Lewis 2002; Xu 2012; Magana et al. 2018), or one may alter the mass–energy evolution equation with bulk viscosity terms based on thermodynamical considerations (see Lima et al. 1988; Brevik et al. 2011; Herrera-Zamorano et al. 2020). Alternatively, the interpretation of SN data may be biased if the observer is located in a local underdense region (e.g., Celerier 2000) or considering that the SN sources tend to be associated with overdensities (e.g., Deledicque 2022).

Yet another possibility, more connected to this work, focuses on the role of matter inhomogeneities and anisotropies that may affect the cosmic expansion due to backreaction or statistical sampling effects (e.g., Buchert & Ehlers 1997; Barausse et al. 2005; Wiltshire 2007; Buchert 2008; Kolb 2011; Buchert & Räsänen 2012; Clifton 2013; Racz et al. 2017; Cosmai et al. 2019; Schander & Thiemann 2021). In fact, on the spatial scales associated with cosmic structures, matter and radiation are expected to be affected by a variety of complex physical processes, including local inhomogeneities, clumping, fractality, anisotropic stresses, gravitational and electromagnetic interactions, tidal torques, inflows and outflows, etc. When investigating background cosmology, one usually does not care about the fine details of such behavior but instead focuses on the description of quantities spatially averaged over sufficiently large scales, where a homogeneous/isotropic Universe is assumed to hold according to the celebrated cosmological principle. But given the nonlinear nature of Einstein’s general relativity equations, it is far from clear to what extent the complex gravitational dynamics on smaller scales can be neglected in modeling the evolution of larger-scale patches and the Universe as a whole.

From an observational perspective, testing homogeneity and isotropy on large scales along cosmic history is not trivial. On the one hand, observations of the CMB show a remarkable consistency with statistical isotropy (meaning that small CMB fluctuations that originated from inflation feature the same power spectrum in different directions on the sky), apart from a few “anomalies” on the largest scales (see Planck Collaboration et al. 2020b; Chiocchetta et al. 2021). On the other hand, it may well be that deviations from homogeneity and isotropy can emerge at later cosmic times, thus requiring them to be checked with different probes at lower redshift. In this vein, many

studies have been conducted exploiting galaxies (see Javanmardi & Kroupa 2017; Sarkar et al. 2019), radio sources (see Bengaly et al. 2019; Siewert et al. 2021; Secrest et al. 2022), gamma-ray bursts (see Tamopolski 2017; Andrade et al. 2019; Ripa & Shafieloo 2019; Horvath et al. 2020), active galactic nuclei (AGN)/quasars (see Gonçalves et al. 2021; Secrest et al. 2021; Friday et al. 2022; Lopez et al. 2022; Tiwari et al. 2023), large-scale bulk flows (see Kashlinsky et al. 2011; Atrio-Barandela et al. 2015; Watkins et al. 2023), HI gas (see Hazra & Shafieloo 2015; Avila et al. 2018, 2023), X-ray emission from galaxy clusters (see Migkas et al. 2020, 2021), and Type Ia SNe (see Javanmardi et al. 2015; Bernal et al. 2017; Colin et al. 2019; Hu et al. 2020; Krishnan et al. 2022; Rahman et al. 2022; Zhai & Percival 2022; McConville & Colgain 2023); the results are still somewhat controversial, with some of these analyses supporting the cosmological principle and others claiming statistically significant deviations from it (see review by Kumar Aluri et al. 2023).

One of the most prominent manifestations of the anisotropic and inhomogeneous nature of the gravitationally driven evolution of the Universe is the progressive appearance of the cosmic web toward late cosmic times. This spider network of quasi-linear structures that permeates the cosmos on large scales is constituted by anisotropic filamentary and planar features (filaments and sheets) intersecting into nodes (knots) where galaxy clusters tend to reside and surrounding large underdense regions (voids) that occupy most of the volume. As shown by numerical simulations, the formation and evolution of the cosmic web are driven by gravitational tidal forces induced by inhomogeneities in the mass distribution and by the multistream migration of matter from adjacent structures (e.g., Springel et al. 2006; Shandarin et al. 2012; Vogelsberger et al. 2014; Libeskind et al. 2018; Martizzi et al. 2019; Wilding et al. 2021; see also Angulo & Hahn 2022).

It is instructive to highlight a few statistical properties of the cosmic web by running an N -body numerical simulation in the standard Λ CDM cosmology, in particular by extracting the distribution of the (over)density field $1 + \delta \equiv \delta\rho/\rho$ smoothed on different coarse-graining scales R . Snapshots of such a simulation at redshift $z \approx 0$ and smoothing scales $R \approx 5\text{--}50\text{--}500 h^{-1}$ Mpc are illustrated in the top panels of Figure 1. Anisotropic/inhomogeneous conditions are manifest for small $R \lesssim$ a few megaparsecs and progressively washed out for larger R , to the point of becoming negligible at scales of $R \gtrsim$ hundreds of megaparsecs, i.e., an appreciable fraction of the current Hubble radius. Interestingly, simulations show that the emergence of the cosmic web via the gravitationally driven growth of structures and voids transforms the statistical distribution of the overdensity field $\Omega \sim 1 + \delta$ from the initial Gaussian to a lognormal shape (even on quasi-linear scales), as also pointed out by theoretical and numerical studies in the literature (e.g., Coles & Jones 1991; Neyrinck et al. 2009; Repp & Szapudi 2017, 2018). Specifically, the average and dispersion of such a lognormal distribution are plotted in the bottom panels of Figure 1 as a function of the smoothing scale and redshift. Moving from larger to smaller scales, the average $\langle \log(1 + \delta) \rangle$ gets progressively biased toward negative values (corresponding to underdense regions, e.g., voids), and the dispersion $\sigma_{\log(1+\delta)}$ increases; the effect is more pronounced toward lower redshifts as structure formation proceeds. From these outcomes, it should be clear that scales smaller than a few megaparsecs are strongly inhomogeneous and anisotropic but

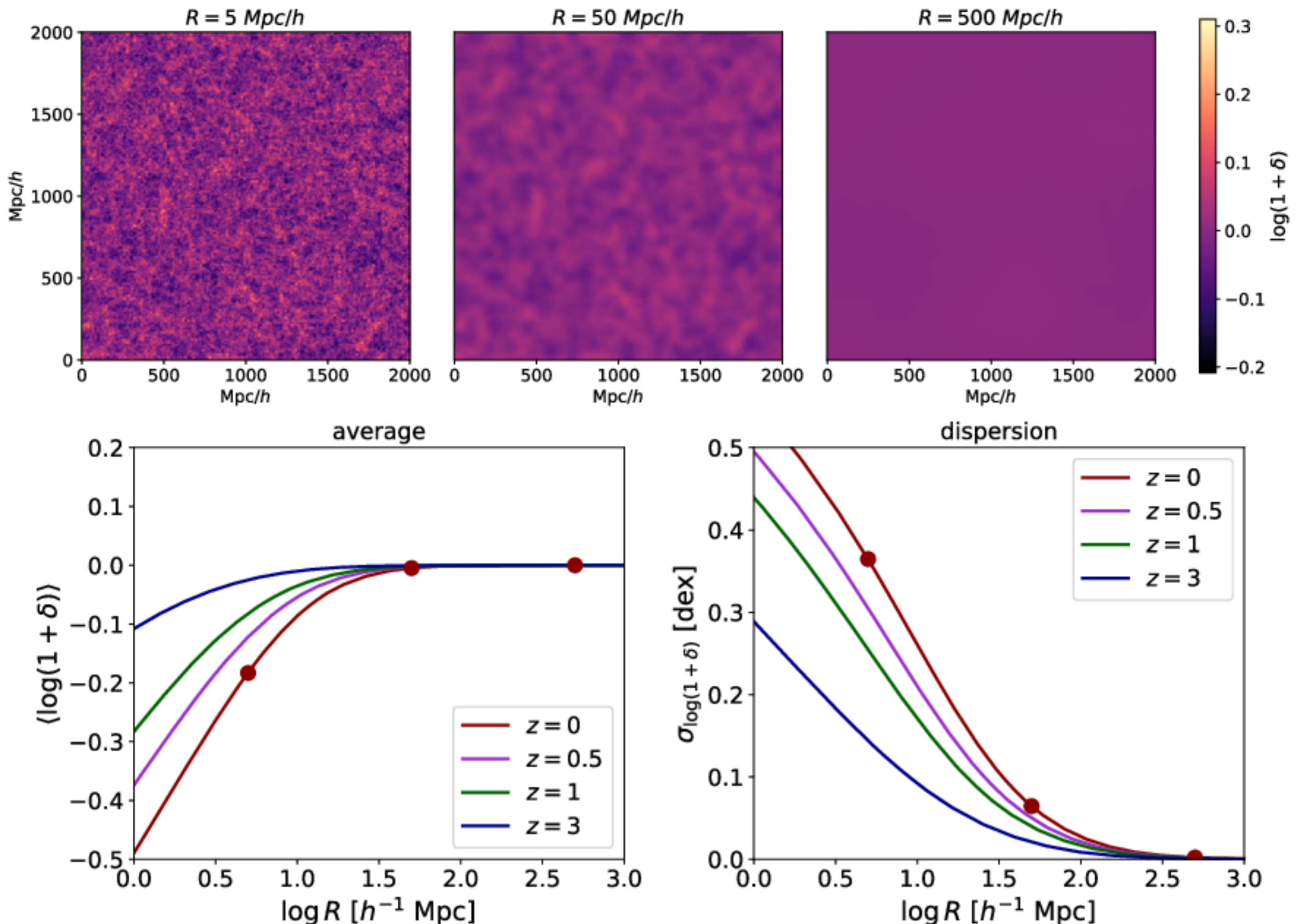


Figure 1. Top panels: snapshots at $z \approx 0$ extracted from an N -body simulation in the Λ CDM cosmology with a box of $2 h^{-1}$ Gpc and 1024^3 particles, which shows the amplitude $\log(1 + \delta)$ of the overdensity field (color-coded) smoothed via a top-hat window function on scales of $R \approx 5$ (left), 50 (middle), and 500 (right) h^{-1} Mpc. Bottom panels: average and dispersion of the lognormal distribution followed by the density contrast field in the simulation when smoothed on different scales R at redshifts $z \approx 0$ (red), 0.5 (magenta), 1 (green), and 3 (blue). The red circles highlight the smoothing scales used in the snapshots shown in the top panels.

dominated by nonlinear structures and peculiar motions detached from the Hubble flow; hence, any major link with the overall cosmic dynamics is presumably lost. At the other end, scales larger than hundreds of megaparsecs are fully homogeneous and isotropic, so that averaging cosmological quantities over them brings about the standard dynamics but at the price of ignoring any possible backreaction effects due to structure formation from the quasi-linear scales of the cosmic web that are still connected to the Hubble flow.

Motivated by the above, in this paper, we focus on scales of tens of megaparsecs associated with the cosmic web and investigate the impact on the cosmic dynamics of the small residual anisotropies/inhomogeneities present there. Our framework is inspired by some of the backreaction models mentioned above, though we attack the problem via a different approach based on stochastic differential equations. This envisages that such patches of the Universe will undergo slightly different evolutions due to local inhomogeneities, matter flows related to anisotropic stresses, tidal forces, gravitational torques, etc. However, we do not aim to follow the details of such a complex dynamics (that would be practically impossible to handle in semianalytic terms) and revert instead to an effective statistical description for the evolution of the various patches in terms of the different

realization of an appropriate noise term in the mass–energy evolution equation. At any given cosmic time, sampling the ensemble of patches will create a nontrivial spatial distribution of the various cosmological quantities, while the overall behavior of the Universe will then be obtained by averaging over the patch ensemble. We assume a simple phenomenological and physically reasonable parameterization of the noise term, tuning it against a wealth of cosmological data sets in the local and high-redshift Universe. We find that, with respect to Λ CDM, in our stochastic model, an accelerated expansion can be enforced at late cosmic times, and the curvature can stay small even in a low-density Universe constituted of matter and radiation; this behavior will ultimately turn out to be due to the nature of the large-scale structure formation, which places far more volume in underdense than in overdense regions, causing the average expansion to skew toward an accelerated behavior. Remarkably, matter can also acquire an effective negative pressure at late times. We also provide predictions for the variance of the cosmological quantities among the different patches as induced by the noise. Finally, we show that our model is capable of solving the Hubble tension and relieving the coincidence problem.

The plan of the paper is as follows. In Section 2, we introduce our cosmological model; in Section 3, we investigate

its implications for the cosmic dynamics; in Section 4, we gauge the noise term against a wealth of cosmological data sets; in Section 5, we examine the time-dependent variance implied by the noise on the cosmological quantities; in Section 6, we explore the future evolution of the Universe; in Section 7; we provide answers to some frequently asked questions; and finally, in Section 8, we summarize our findings and outline future perspectives.

2. Basic Setup

We consider a Universe composed of (baryonic+dark) matter and radiation, subject to the laws of canonical general relativity. We focus on patches of order tens of megaparsecs, where the local density field is unbiased with respect to the average density of the Universe (i.e., $\langle \log(1 + \delta) \rangle \approx 0$), but residual small anisotropies/inhomogeneities associated with the cosmic web are present (see Section 1 and Figure 1). In these conditions, we assume that the standard Friedmann–Robertson–Walker metric can be applied to a good approximation (as also shown by detailed GR simulations; see Räsänen 2010; Koksang 2019; Macpherson et al. 2019; Adamek et al. 2019). Yet any of such patches of the Universe will experience slightly different evolutions along cosmic history due to local inhomogeneities, matter flows induced by anisotropic stresses, tidal forces, and other complex gravitational processes that for all practical purposes are extremely difficult to model ab initio or handle (semi)analytically. Therefore, we revert to a statistical description in terms of stochastic differential equations, phenomenologically characterizing the different evolution of the patches as a function of cosmic time via the diverse realizations of a noise term; meanwhile, at any given cosmic time, sampling the ensemble of patches will create a nontrivial spatial distribution of the various cosmological quantities. Finally, the overall behavior of the Universe at any cosmic time will be obtained by averaging over the patch ensemble.

Technically, we add a simple stochastic term to the mass–energy evolution equation with the following properties (see also Section 7 for an extended discussion): stochasticity is driven by Gaussian white noise, $\eta(t)$; the stochastic term scales proportionally to the energy density of each component, so that the linearity of the mass–energy evolution equation is preserved; and the stochastic term features an inverse power-law dependence on the Hubble parameter, so that at early times, random effects become negligible, in order to be consistent with the statistical isotropy of the CMB. The evolution of each different patch of the Universe is described by the diverse realizations of the noise term $\eta(t)$ via the system of stochastic differential equations (in the Stratonovich sense; see Appendix A),

$$\begin{cases} H^2 = \frac{8\pi G}{3} (\rho_m + \rho_\gamma) - \frac{\kappa c^2}{a^2}, \\ \dot{\rho}_{m,\gamma} = -3 H \rho_{m,\gamma} (1 + w_{m,\gamma}) + \zeta \rho_{m,\gamma} \sqrt{H_*} \left(\frac{H}{H_*}\right)^\alpha \eta(t); \end{cases} \quad (1)$$

here G is the standard gravitational constant, c is the speed of light, $a(t)$ is the scale factor normalized to unity at the present time, $H(t) \equiv \dot{a}/a$ is the Hubble rate, $H_* \equiv 100 \text{ km s}^{-1} \text{ Mpc}^{-1}$ is a reference value, κ is the curvature constant, and $\rho_{m,\gamma}$ is the energy density of matter and radiation with equation-of-state

parameters $(w_m; w_\gamma) = (0; 1/3)$. In addition, as mentioned above, $\eta(t)$ is Gaussian white noise (physical dimensions $1/\sqrt{t}$) with ensemble-averaged properties $\langle \eta(t) \rangle = 0$ and $\langle \eta(t)\eta(t') \rangle = 2 \delta_D(t - t')$, and $(\zeta \geq 0; \alpha \leq 0)$ are two parameters regulating the strength and redshift dependence of the noise that are yet to be specified (these will be set by comparison with cosmological observables; see Section 4). Note that when introducing the normalized Hubble rate $h \equiv H/H_*$ and the density parameters $\Omega_{m,\gamma} \equiv 8\pi G \rho_{m,\gamma} / 3H^2$, the Friedmann equation just reads $\Omega_\kappa \equiv -\kappa c^2 / a^2 h^2 = 1 - \Omega_m - \Omega_\gamma$.

The multiplicative factor in front of the Gaussian white noise η is an ansatz inspired by the following naive argument. As it occurs in Λ CDM (see Figure 1), one expects that at late times, the overdensity $1 + \delta \propto \rho$ smoothed on a certain coarse-graining scale (e.g., tens of megaparsecs) constitutes a random field following a lognormal distribution (see the theoretical arguments by Coles & Jones 1991; see also Neyrinck et al. 2009; Repp & Szapudi 2017, 2018). In simple words, sampling patches of the present Universe at different spatial locations yields a lognormal distribution for ρ or, equivalently, a normal distribution for $\log \rho$. In terms of basic stochastic processes, such a distribution would be naturally created by an ensemble of regions whose density evolves stochastically in time under Gaussian white noise $\eta(t)$ or, in other words, for which $d_t \log \rho \sim \dot{\rho}/\rho \propto \eta(t)$, with the proportionality constant being related to the variance of the density distribution (see Risken 1996; Paul & Baschnagel 2013; see also Appendix A). Although Equation (1) describes a more complex stochastic system (since the second equation features a dilution term, and it is coupled to the first via the Hubble parameter), this analogy has inspired us to adopt a noise term $\dot{\rho} \sim \zeta H^\alpha \rho$, with the parameters ζ and α describing our ignorance of the present value and the redshift evolution of the variance in the density distribution for a generic cosmology that can, in principle, be different from Λ CDM.

We stress that Equation (1) should be meant to hold on patches of the Universe with a typical smoothing (or coarse-graining) scale that constitutes in itself a hidden parameter of the model, though in turn fully determined by the noise and cosmological ones. Such a scale will be estimated after setting the noise and cosmological parameters via comparison with data (Section 4.1) and evaluating the typical fluctuations of the density field induced by the noise (Section 5); here we anticipate that it will turn out to be around tens of megaparsecs, a typical size associated with the cosmic web. In the same perspective, notice that the noise term in Equation (1) subtends deviations from local energy conservation in different patches of the Universe with a size given by the aforementioned coarse-graining scale that can be associated with, e.g., matter flows; given the number of fluctuations in the density field induced by the noise as computed in Section 5, these deviations will turn out to be minor.

Finally, note that the noise term has a natural timescale t_η associated with it that can be easily derived by dimensional analysis of the second term on the right-hand side of the mass–energy evolution equation above; writing $\dot{\rho} \sim \rho/t_\eta$ and $\eta \sim 1/\sqrt{t_\eta}$, one finds $t_\eta \sim 1/(H_* \zeta^2 h^{2\alpha})$. This has to be compared with the typical timescale of deterministic dilution expressed by the first term on the right-hand side of the same equation, e.g., for matter $t_{\text{exp}} \sim 1/(3H)$. The competition

between noise and dilution can be quantified by the ratio $t_\eta/t_{\text{exp}} \sim 3/(\zeta^2 h^{2\alpha-1})$, which will be evaluated in Section 4.1 after having determined the noise and cosmological parameters via comparison with data.

Hereafter, we will refer to this model of the Universe as η CDM, since η is the standard mathematical symbol for the noise ruling its dynamics. Although constituting a seemingly simple modification to the standard cosmological framework, our proposal has relevant implications for cosmic history. Three preliminary remarks are in order. First, since Equations (1) above are coupled, not only $\rho_{m,\gamma}$ but also the quantities a and H are promoted to stochastic variables; these will fluctuate in time under the action of the noise in a slightly different way for each of the patches (corresponding to different noise realizations). This is better highlighted by combining Equations (1) to obtain the acceleration equation,

$$\frac{\ddot{a}}{a} = -\frac{4\pi G}{3}(\rho_m + 2\rho_\gamma) + \zeta \frac{4\pi G}{3\sqrt{H_*}}(\rho_m + \rho_\gamma) \left(\frac{H}{H_*}\right)^{\alpha-1} \eta(t), \quad (2)$$

implying that the noise term acts as a random fluctuation onto the dynamics in each patch of the Universe; plainly, posing $\zeta=0$ yields the usual acceleration equation. Therefore, under the influence of the noise, each patch of the Universe will undergo a slightly different evolution in cosmic time; meanwhile, at any given cosmic time, sampling the ensemble of patches will create a nontrivial spatial distribution of the various cosmological quantities. Second, note that the noise term is “multiplicative,” meaning that it depends on the system state; as $\eta(t)$ fluctuates, the variables $\rho_{m,\gamma}$ and H appearing in the stochastic term also vary. Therefore, in Equation (2), one finds that $\langle \rho_{m,\gamma} H^{\alpha-1} \eta \rangle$ is not null even if $\langle \eta \rangle$ is; the result will be a noise-induced drift affecting the late-time ensemble-averaged cosmological evolution (actually accelerating it, as shown in Section 3).

Third, it is plain that the overall cosmic dynamics will be specified not only by the above equations but also by sensible boundary conditions. Since the noise term is, by construction, negligible at early times, the evolution should mirror that of a standard cosmological model in the remote past. Then one may envisage integrating the stochastic system forward in cosmic time from such initial conditions; however, this procedure cannot be correct, since it would possibly create an uncontrolled diffusion of the cosmological quantities toward the present to values that, in principle, may be very far from the spatially average ones or even nonphysical in some intermediate step of cosmic history. To avoid the issue, one must require that the values of the cosmological quantities measured by an observer here and now are close to the average values; this means that the overall evolution cannot be a simple diffusion but rather a diffusion bridge, i.e., a controlled diffusion such that the initial and final values of the different random paths are appropriately assigned (we anticipate that the final values will be set by comparison with cosmological data and the initial one by integrating back in time the equations describing the average evolution; more on this below). Diffusion bridges have recently found many applications ranging from genetics, to economics, to data science (see Pedersen 1995; Durham & Gallant 2002; Delyon & Hu 2006; Lindstrom 2012; Bladt & Sørensen 2014; Whitaker et al. 2017;

Heng et al. 2022). The treatment of such conditioned diffusion problems is not trivial at all (especially when drift terms are present), and exact solutions are practically impossible to obtain except for very peculiar setups; however, various techniques have been developed to find approximate solutions in general cases, as exploited below.

Before proceeding, it is convenient to put Equation (1) in a more transparent and numerically tractable form. First of all, we differentiate the Friedmann equation, reexpress the term $\kappa c^2/a^2$ in terms of H and $\rho_{m,\gamma}$, exploit the mass–energy evolution equations to explicitly write $\dot{\rho}_{m,\gamma}$, and then use $\dot{\Omega}_{m,\gamma}/\Omega_{m,\gamma} = \dot{\rho}_{m,\gamma}/\rho_{m,\gamma} - 2\dot{h}/h$ to obtain an equation for the density parameters $\Omega_{m,\gamma}$. Finally, we introduce the normalized Hubble rate $h \equiv H/H_*$ and redefine the time variable $\tau \equiv H_* t$ such that $\eta(t) \rightarrow \eta(\tau)\sqrt{H_*}$ by the property of the Gaussian noise. All in all, we get (an overdot means differentiation with respect to τ)

$$\begin{cases} \dot{h} = h^2 \left(-1 - \frac{\Omega_m}{2} - \Omega_\gamma\right) + \frac{\zeta}{2}(\Omega_m + \Omega_\gamma) h^{\alpha+1} \eta(\tau) \\ \dot{\Omega}_m = \Omega_m h \left(-1 + \Omega_m + 2\Omega_\gamma\right) + \zeta(1 - \Omega_m - \Omega_\gamma) \Omega_m h^\alpha \eta(\tau) \\ \dot{\Omega}_\gamma = \Omega_\gamma h \left(-2 + \Omega_m + 2\Omega_\gamma\right) + \zeta(1 - \Omega_m - \Omega_\gamma) \Omega_\gamma h^\alpha \eta(\tau), \end{cases} \quad (3)$$

supplemented by the final boundary values $(h_0, \Omega_{m,0}, \Omega_{\gamma,0})$ at the present time τ_0 . Plainly, for $\zeta=0$, the usual dynamics of a (nonzero curvature) patch of the Universe is recovered. As mentioned above, in principle, a stochastic system just characterized by a terminal boundary value is ill defined, since the randomness naturally develops with the evolution proceeding forward in time. However, in the present context, the problem is made meaningful by the temporal behavior of the noise term, which makes fluctuations negligible at early times, to imply that the full stochastic solutions must converge in the remote past to the spatially average one (i.e., obtained at each cosmic time by averaging over the patch ensemble). Thus, the technique to solve the problem (mutated by Whitaker et al. 2017; details in Appendix B) is to separate the stochastic variables $(h; \Omega_m; \Omega_\gamma) = (\bar{h} + \tilde{h}; \bar{\Omega}_m + \tilde{\Omega}_m; \bar{\Omega}_\gamma + \tilde{\Omega}_\gamma)$ in an average (barred variables) and a residual random (tilded variables) component. On the one hand, the average behavior can be shown to satisfy an ordinary differential equation that is easily solved backward in time from the terminal condition at τ_0 to provide an initial condition at a time $\tau_{\text{in}} \ll \tau_0$ for the full system; remarkably, this equation inherits a noise-induced drift term that will have relevant consequences on the late-time cosmic dynamics (see next section). On the other hand, the residual random component will render the fluctuations of the various patches and create variance in the (spatial) distribution of the cosmological quantities at a given cosmic time. Such a random component can be shown to satisfy a stochastic equation (actually also requiring the average solution as an input) that can be integrated forward in time from an initial null value at τ_{in} ; moreover, this equation features a spurious drift term that forces the solution to hit a null terminal value at τ_0 , i.e., to execute a diffusion bridge (see Appendix B for details). All in all, the overall stochastic process will be characterized by well-defined initial and final values connected by the average evolution plus some random behavior at intermediate times.

In the next sections, we will apply such a technique to Equation (3) to investigate the cosmic dynamics, set the terminal conditions and noise parameters by comparison with cosmological observables, and estimate the variance in the evolution of the different patches as induced by the noise term.

3. Average Evolution

The equations ruling the ensemble-averaged behavior $(\bar{h}, \bar{\Omega}_m, \bar{\Omega}_\gamma)$ in the evolution of Equation (3) can be derived from the procedure outlined in Appendix A. After some tedious algebra, we obtain

$$\begin{cases} \dot{\bar{h}} = \bar{h}^2 \left(-1 - \frac{\bar{\Omega}_m}{2} - \bar{\Omega}_\gamma \right) + \frac{\zeta^2}{2} (\bar{\Omega}_m + \bar{\Omega}_\gamma) \bar{h}^{2\alpha+1} \left[1 - \frac{1-\alpha}{2} (\bar{\Omega}_m + \bar{\Omega}_\gamma) \right] \\ \dot{\bar{\Omega}}_m = \bar{\Omega}_m \bar{h} (-1 + \bar{\Omega}_m + 2\bar{\Omega}_\gamma) + \zeta^2 (1 - \bar{\Omega}_m - \bar{\Omega}_\gamma) \bar{\Omega}_m \bar{h}^{2\alpha} \left[1 - \frac{4-\alpha}{2} (\bar{\Omega}_m + \bar{\Omega}_\gamma) \right] \\ \dot{\bar{\Omega}}_\gamma = \bar{\Omega}_\gamma \bar{h} (-2 + \bar{\Omega}_m + 2\bar{\Omega}_\gamma) + \zeta^2 (1 - \bar{\Omega}_m - \bar{\Omega}_\gamma) \bar{\Omega}_\gamma \bar{h}^{2\alpha} \left[1 - \frac{4-\alpha}{2} (\bar{\Omega}_m + \bar{\Omega}_\gamma) \right], \end{cases} \quad (4)$$

where, on the right-hand side, the second addenda are the noise-induced drift terms stemming from the multiplicative nature of the noise; in fact, the average evolution is informed on and affected by the noise of the original stochastic process. This system of equations may be easily solved backward in cosmic time from terminal conditions at the present epoch τ_0 given by $(h_0; \Omega_{m,0}; \Omega_{\gamma,0})$ to yield the average evolution of the Hubble rate and density parameters across cosmic history. We are now ready to point out that the dynamics implied by Equation (4) has three relevant consequences.

1. *Late-time acceleration without dark energy.* One can derive the deceleration parameter q from the first of Equations (4), to read $\dot{\bar{h}}/\bar{h}^2 \equiv -(1 + q)$. At late times, one can neglect radiation ($\bar{\Omega}_\gamma \ll \bar{\Omega}_m$) so that

$$\bar{q} = -1 - \frac{\dot{\bar{h}}}{\bar{h}^2} = \frac{\bar{\Omega}_m}{2} - \frac{\zeta^2}{2} \bar{\Omega}_m \bar{h}^{2\alpha-1} \left(1 - \frac{1-\alpha}{2} \bar{\Omega}_m \right); \quad (5)$$

whenever $\bar{\Omega}_m \lesssim 2/(1-\alpha)$, the stochastic term tends to reduce the deceleration parameter expected from a standard open cosmology without dark energy, and for appropriate values of α and ζ , an accelerated expansion with $q < 0$ at late times can be enforced. The physical interpretation of this effect is that the overall ensemble of patches tends to drift toward an evolution dominated by low-density regions (see also Section 7). High-order cosmographic quantities can be easily computed from the expression above (e.g., Visser 2005); e.g., the jerk parameter is given by

$$\bar{j} = 1 + 3 \frac{\dot{\bar{h}}}{\bar{h}^2} + \frac{\ddot{\bar{h}}}{\bar{h} \bar{h}^3} = \bar{q} + 2 \bar{q}^2 - \frac{\dot{\bar{q}}}{\bar{h}} \quad (6)$$

and will be shown to have a nontrivial evolution at late cosmic times.

2. *Small curvature in a low-density Universe.* One can derive the average evolution of the global effective curvature $\bar{\Omega}_\kappa$ along the following lines. By combining Equations (4) after some algebraic manipulation, one gets

$$\frac{2\dot{\bar{h}}}{\bar{h}} = \frac{\dot{\bar{\Omega}}_m + \dot{\bar{\Omega}}_\gamma}{1 - \bar{\Omega}_m - \bar{\Omega}_\gamma} - 2\bar{h} + \frac{3}{2} \zeta^2 \bar{h}^{2\alpha} (\bar{\Omega}_m + \bar{\Omega}_\gamma)^2. \quad (7)$$

Formally integrating in time (recall that $\bar{h} dt = d \ln \bar{a}$ in terms of the scale factor) and recognizing that the integration constant is related to the curvature parameter $\bar{\Omega}_\kappa \propto -\kappa/\bar{h}^2 \bar{a}^2$, one obtains the modified Friedmann constraint,

$$\bar{\Omega}_\kappa = (1 - \bar{\Omega}_m - \bar{\Omega}_\gamma) \times \exp \left[-\frac{3}{2} \zeta^2 \int d \ln \bar{a} \bar{h}^{2\alpha-1} (\bar{\Omega}_m + \bar{\Omega}_\gamma)^2 \right]. \quad (8)$$

Equation (8) directly implies that $\bar{\Omega}_\kappa$ is negligible in the remote past, since the exponential term containing the

noise parameters tends to 1, and $\bar{\Omega}_m + \bar{\Omega}_\gamma \approx 1$ applies like in the standard Λ CDM cosmology. However, $\bar{\Omega}_\kappa$ starts growing toward the present, then attains a maximum value $\bar{\Omega}_\kappa \lesssim 0.1$ at the time when $\bar{h} \approx [\zeta^2 (1 - (1-\alpha)\bar{\Omega}_m/2)]^{1/(1-2\alpha)}$ and eventually decreases again toward zero in the infinite future. On the one hand, such an evolution is consistent with inflationary scenarios, which predict that any possible initial curvature has already been erased via a super-exponential expansion at a time of around 10^{-32} s after the Big Bang (see Efstathiou & Gratton 2020); on the other hand, the noise induces, via Equation (8), a nontrivial evolution of the curvature parameter implying modest deviations from flatness around the cosmic times where the acceleration sets in that could possibly constitute a specific test of the η CDM model in the future. All in all, for appropriate values of ζ and α , the curvature parameter $\bar{\Omega}_{\kappa,0}$ may, at present, be appreciably reduced to small values, even in a low-density matter-dominated Universe.

3. *Matter with negative pressure at late times.* One can derive the effective equation of state for the matter component at late times from the first two of Equations (4); neglecting radiation and coming back to the volume energy density via $\dot{\bar{\rho}}_m/\bar{\rho}_m = \dot{\bar{\Omega}}_m/\bar{\Omega}_m + 2\dot{\bar{h}}/\bar{h}$, one has

$$\begin{aligned} \dot{\bar{\rho}}_m &= -3 \bar{h} \bar{\rho}_m + \frac{\zeta^2}{2} \bar{h}^{2\alpha} \\ &\times \bar{\rho}_m [2 - (4 - \alpha)\bar{\Omega}_m + 3\bar{\Omega}_m^2]. \end{aligned} \quad (9)$$

Then, introducing an effective equation-of-state parameter \bar{w}_m such that $\dot{\bar{\rho}}_m = -3 \bar{h} \bar{\rho}_m (1 + \bar{w}_m)$, one can write

$$\bar{w}_m = -\frac{\zeta^2}{6} \bar{h}^{2\alpha-1} [2 - (4 - \alpha)\bar{\Omega}_m + 3\bar{\Omega}_m^2]; \quad (10)$$

this plainly tends to the standard $\bar{w}_m \approx 0$ at early times, while values $\bar{w}_{m,0} < 0$ can apply toward the present, implying that matter effectively behaves as a negative pressure component. However, note from Equation (5) that

in η CDM, the condition $\bar{w}_m < -1/3$ (e.g., violation of the strong-energy condition in general relativity) is not required to enforce cosmic acceleration.

4. Tuning the Noise

Now we move to determine the terminal conditions and the parameters ($\zeta; \alpha$) regulating the noise strength and redshift dependencies by comparing the evolution implied by Equation (4) with the data. Since the early evolution of the Universe in the η CDM and Λ CDM models is indistinguishable (noise is negligible at early times), for the sake of simplicity, we set the radiation energy density parameter $\Omega_{\gamma,0} h_0^2 \approx 2.47 \times 10^{-5}$ to the value measured by the Planck mission (Planck Collaboration et al. 2020a) and the baryon density $\Omega_{b,0} h_0^2 \approx 0.0222$ to the value suggested by Big Bang Nucleosynthesis constraints (Aver et al. 2015). Then our cosmological model will be characterized by the parameter sets ($h_0; \Omega_{m,0}; \zeta; \alpha$) that we determine by fitting a number of observables in the local and distant Universe; specifically, we consider the following data sets.

1. *Type Ia SNe with Cepheid zero-point calibration.* We exploit the Pantheon+ sample of ≈ 1700 Type Ia SNe in the redshift range $z \sim 0.001$ –2.3 with Cepheid zero-point calibration from the SH0ES team (Brout et al. 2022; Riess et al. 2022; Scolnic et al. 2022) to fit for the distance modulus $\mu(z) = 5 \log(D_L/\text{Mpc}) + 25$, where the luminosity distance in a positively curved Universe is computed as

$$D_L(z) = \frac{c(1+z)}{H_0 \sqrt{\Omega_{m,0}}} \sinh \left[\sqrt{\Omega_{m,0}} \int_0^z dz' \frac{H_0}{H(z')} \right]. \quad (11)$$

The full covariance matrix of the Pantheon+ data has been exploited (this includes statistical and systematic uncertainties in the distance modulus and Cepheid host covariance).

2. *CMB first peak angular scale.* We require the model to reproduce the angular scale of the first peak in the CMB temperature spectrum $\theta_* \approx r_*/D_M(z_*)$ as measured by the Planck Collaboration (2020a); here r_* is the comoving sound horizon at recombination, and $D_M(z_*)$ is the transverse comoving distance at the recombination redshift z_* . We use the approximations $z_*(h_0, \Omega_{m,0}, \Omega_{b,0})$ and $r_*(h_0, \Omega_{m,0}, \Omega_{b,0})$ by Hu & Sugiyama (1996).
3. *BAOs.* We exploit 18 data points in the redshift range $z \sim 0.1$ –2.4 from various BAO isotropic measurements (Beutler et al. 2011; Kazin et al. 2014; Ross et al. 2015; Alam et al. 2017; Ata et al. 2018; du Mas des Bourboux et al. 2020; Bautista et al. 2021; de Mattia et al. 2021; Hou et al. 2021; Raichoor et al. 2021; Zhao et al. 2022) and fit for the ratio $r_d/D_V(z)$ between the sound horizon at the drag epoch z_d and the angle-averaged galaxy BAO measurement $D_V(z) = [cz D_M^2(z)/H(z)]^{1/3}$, where $D_M(z) = D_L(z)/(1+z)$ is the transverse comoving distance. We also consider the ratio between the Hubble distance and the sound horizon at the drag epoch $c/H(z)r_d$ inferred from transverse BAO $_{\perp}$ measurements (see Alam et al. 2017; du Mas des Bourboux et al. 2020; Bautista et al. 2021; de Mattia et al. 2021; Hou et al. 2021), properly taking into account the covariance with some of the isotropic measurements mentioned above. We use the approximations $z_d(h_0, \Omega_{m,0}, \Omega_{b,0})$ and $r_d(h_0, \Omega_{m,0}, \Omega_{b,0})$

by Aubourg et al. (2015); see also Eisenstein & Hu 1998).

4. *Cosmic chronometers (CCs).* We also consider the redshift-dependent Hubble parameter $H(z)$ as determined from differential ages of early-type galaxies; the data set includes 33 data points in the redshift range $z \sim 0.07$ –2.4 from various authors (see Simon et al. 2005; Stern et al. 2010; Moresco et al. 2012a, 2012b, 2016; Zhang et al. 2014; Moresco 2015; Ratsimbazafy et al. 2017; Borghi et al. 2022; Jiao et al. 2023). We use the full covariance matrix, taking into account modeling uncertainties, mainly related to the choice of the initial mass function, of stellar libraries and stellar population synthesis models (see Moresco et al. 2022 for details). Notice that this data sets is characterized by considerable systematic and statistical uncertainties and, as such, will not crucially impact the determination of cosmological parameters.
5. *Age of globular clusters.* We include the latest estimate on the age of the Universe from globular cluster dating (Valcin et al. 2021); however, since the latter still has large statistical uncertainties (and may be affected by several systematics), we also include a hard lower bound of $\gtrsim 11$ Gyr to the age of the Universe from classic globular cluster age constraints (e.g., Krauss & Chaboyer 2003).

For parameter inference, we exploit a Bayesian Markov Chain Monte Carlo (MCMC) framework, numerically implemented via the Python package `emcee` (Foreman-Mackey et al. 2013). We use a standard Gaussian likelihood $\mathcal{L}(\theta) \equiv -\sum_i \chi_i^2(\theta)/2$, where $\theta = \{h_0; \Omega_{m,0}; \zeta; \alpha\}$ is the vector of the parameters, and the summation is over different observables; for the latter, the corresponding $\chi_i^2 = \sum_j [\mathcal{M}(z_j, \theta) - \mathcal{D}(z_j)]^2 / \sigma_{\mathcal{D}}^2(z_j)$ is obtained by comparing our empirical model expectations $\mathcal{M}(z_j, \theta)$ to the data $\mathcal{D}(z_j)$ with their uncertainties $\sigma_{\mathcal{D}}^2(z_j)$, summing over the different redshifts z_j of the data points (when necessary, we take into account the full covariance matrix of the observables). We adopt flat priors $\pi(\theta)$ on the parameters within the ranges $h_0 \in [0, 1]$, $\Omega_{m,0} \in [0, 1]$, $\zeta \in [0, 3]$, and $\alpha \in [-3, 1]$. We then sample the posterior distribution $\mathcal{P}(\theta) \propto \mathcal{L}(\theta)\pi(\theta)$ by running `emcee` with 10^4 steps and 100 walkers; each walker is initialized with a random position uniformly sampled from the (flat) priors. To speed up convergence, we adopt a mixture of differential evolution (see Nelson et al. 2014) and `snooker` (see ter Braak & Vrugt 2008) moves of the walkers in proportions of 0.8 and 0.2, respectively. After checking the autocorrelation time, we remove the first 20% of the flattened chain to ensure the burn-in; the typical acceptance fractions of the various runs are around 30%–40%.

4.1. Fitting Results

The outcomes of the fitting procedure are illustrated in the corner plot of Figure 2. The colored contours are the 1σ – 2σ – 3σ confidence intervals of the posterior for the analysis based on the different data sets: SN+Cepheid (blue), CC+transverse BAO $_{\perp}$ (red), BAO+CMB θ_* (green), and joint analysis (black); the white crosses are the best-fit positions of the joint analysis, and in the diagonal panels, the marginalized distributions of the various parameters for the joint analysis are also shown. The marginalized constraints are summarized in Table 1, where the reduced χ_r^2 of the fits are also reported.

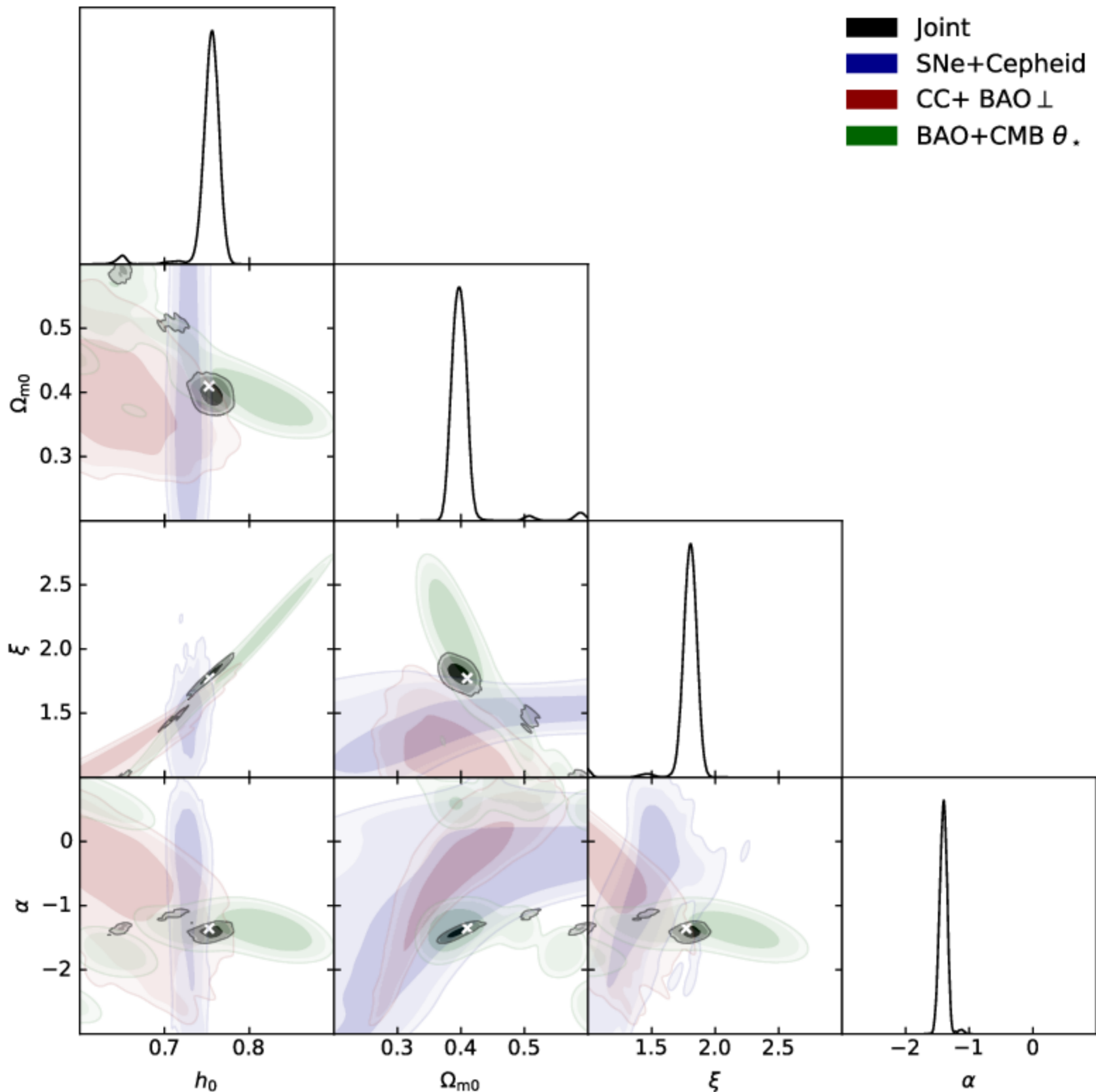


Figure 2. MCMC posterior distributions in the η CDM model for the normalized Hubble constant h_0 , the matter density parameter $\Omega_{m,0}$, and the parameters regulating the noise strength ζ and time dependence α . Colored contours/lines refer to different observables: blue for SN+Cepheid, orange for CC+transverse BAO $_{\perp}$, green for BAO+CMB first peak angular position, and black for joint analysis. The contours show 1σ – 2σ – 3σ confidence intervals, white crosses mark the maximum-likelihood estimates of the joint analysis, and the marginalized distributions of the joint analysis are reported in the diagonal panels in arbitrary units (normalized to 1 at their maximum value).

The joint analysis robustly constrains all of the parameters of the η CDM model. As expected, the value of h_0 is mainly set by SN+Cepheid and BAO+CMB, with the former strongly contributing to reducing the overall uncertainty. It must be stressed that in the η CDM model, at variance with standard Λ CDM, no h_0 tension exists, in that the determinations from SN+Cepheid and BAO+CMB are consistent within 2σ , with BAO+CMB preferring slightly larger values. There is instead a tendency for CC+BAO $_{\perp}$ to give slightly smaller value of h_0 (though still marginally consistent within 3σ), but the larger uncertainties on such a data set do not impact the joint analysis much. As to $\Omega_{m,0}$, the joint analysis is dominated by the constraint from BAO+CMB that tends to require a universe with a small average curvature. On the one hand, this does not permit too-low values of $\Omega_{m,0}$, which is indeed larger than ≈ 0.3 at 3σ ; on the other hand, the noise term acting in Equation (8)

allows for values of $\Omega_{m,0} \approx 0.4$ appreciably smaller than 1 at the price of enhancing the noise strength ζ or setting an appropriate negative value of the parameter α regulating the time dependence of the noise. In particular, the latter is mainly determined by BAO+CMB data that can actually probe, though in an integrated way, the conditions in the early Universe; the noise strength ζ is also appreciably constrained by SN cosmography, as shown by Equation (5).

Recall from Section 2 that the relative importance of noise and dilution terms in the mass–energy evolution equation (second of Equations (1)) is quantified by the ratio $t_{\eta}/t_{\text{exp}} \sim 3/(\zeta^2 h^{2\alpha-1})$; using the best-fit values of the noise and cosmological parameters, we can now evaluate that it is very large (noise is negligible) at high redshift, it crosses unity (i.e., noise starts to dominate and cosmic acceleration kicks in) at $z \approx 0.6$, and it amounts to $\sim 1/3$ at the present time.

Table 1Marginalized Posterior Estimates in Terms of Mean and 1σ Confidence Interval (and Best-fit Value) for the Fits with the η CDM Model to Different Cosmological Data Sets, as Listed in the First Column

| Data Set | h_0 | $\Omega_{m,0}$ | ζ | α | χ_r^2 |
|-------------------|----------------------------------|----------------------------------|-------------------------------|---------------------------------|------------|
| Joint | $0.752^{+0.012}_{-0.005}$ [0.75] | $0.403^{+0.005}_{-0.018}$ [0.40] | $1.78^{+0.08}_{-0.03}$ [1.77] | $-1.41^{+0.07}_{-0.07}$ [-1.36] | 0.44 |
| SN+Cepheid | $0.73^{+0.01}_{-0.01}$ [0.73] | $0.47^{+0.14}_{-0.27}$ [0.40] | $1.45^{+0.20}_{-0.13}$ [1.44] | $-0.74^{+1.10}_{-0.48}$ [-0.96] | 0.29 |
| CC+BAO $_{\perp}$ | $0.64^{+0.05}_{-0.05}$ [0.64] | $0.39^{+0.06}_{-0.06}$ [0.39] | $1.14^{+0.20}_{-0.20}$ [1.20] | $-0.48^{+0.71}_{-0.44}$ [-0.41] | 0.46 |
| BAO+CMB | $0.76^{+0.11}_{-0.22}$ [0.84] | $0.42^{+0.06}_{-0.06}$ [0.38] | $1.69^{+0.50}_{-1.69}$ [2.31] | $-1.13^{+0.50}_{-0.50}$ [-1.38] | 1.57 |

Note. Other columns report the values of the normalized Hubble constant h_0 , present matter energy density $\Omega_{m,0}$, noise strength ζ , noise redshift dependence α , and reduced χ_r^2 of the various fits. We set the radiation density $\Omega_{\gamma,0} h_0^2 \approx 2.47 \times 10^{-5}$ to the value measured by the Planck mission (Planck Collaboration et al. 2020a) and the baryon density $\Omega_{b,0} h_0^2 \approx 0.0222$ to the value suggested by Big Bang Nucleosynthesis constraints (Aver et al. 2015); a hard bound on the age of the Universe at 11 Gyr was placed.

In Figure 3, we illustrate how the η CDM model performs on the fitted observables. In each panel, the median (solid lines) and 2σ credible intervals (shaded areas) from sampling the posterior distribution of the joint analysis are shown; for reference, we also report (dashed lines) the median for the analysis of the individual observables. The individual fits are very good in all cases. The joint analysis fit performs decently on all the observables, being consistent with all of the data points within 2σ ; the most evident discrepancy is with the determinations of the Hubble constant from CC+BAO $_{\perp}$, though the large error bars of these data points impact marginally on the overall goodness of the fit. However, it should be stressed that the majority of the CC data reported in the figure and exploited for the fit have been derived based on the Bruzual & Charlot (2003) stellar population synthesis libraries; it is known (see Moresco et al. 2022) that using the Maraston & Stromback (2011) models instead yields values of $H(z)$ that are systematically higher, especially toward higher z .

In Figure 4, we illustrate the evolution of the best-fit η CDM Universe from the joint analysis; for reference, a flat Λ CDM and an open CDM model with the same values of $h_0 \approx 0.75$ and $\Omega_{m,0} \approx 0.4$ are also reported for comparison. The top panel shows the evolution of the Hubble parameter, with the inset zooming in on the late-time Universe. The behavior of our η CDM model closely mirrors the standard Λ CDM while progressively departing from an open model toward the present; this is because cosmic acceleration sets in with the right timing, and the average curvature stays small despite the rather low matter density. The middle panel displays the evolution of the energy density parameters for the various components. At high redshift, all models are indistinguishable, since matter (blue) and radiation (orange) dominate the early-time evolution, and the noise is negligible. Moving toward lower redshifts, the open model departs from the other two, since curvature (green) begins to grow early on, while the η CDM and Λ CDM models are similar. Spatial flatness in Λ CDM is ensured by the presence of the additional dark energy component (red), while in η CDM, the curvature is kept to low values (though not null) by the noise-induced drift term in Equation (8). In the middle panel, for reference, the green shaded area on the η CDM curvature parameter illustrates the typical 2σ uncertainty on the energy densities. The inset focuses on the evolution of the equation-of-state parameter \bar{w} for the dominant component at late times; an open universe is dominated by curvature with constant $\bar{w} = -1/3$, the Λ CDM

model is dominated by dark energy with $\bar{w} = -1$ (generalizations are obviously possible), and the η CDM model is dominated by matter with an evolving \bar{w} given by Equation (10), which is zero at early times, grows slightly positive, attains a maximum, and then decreases to negative values toward the present.

The bottom panel illustrates relevant cosmological time-scales, namely, the age of the Universe (cyan) and the look-back time (magenta) as a function of redshift; the η CDM and Λ CDM are almost indistinguishable, with an age approximately given by $1/H_0$, while the open model is clearly younger, since it lacks the cosmic acceleration phase at late times. The inset displays the deceleration parameter q and jerk j . The former is positive for the open model, which is decelerating, while it assumes similar negative values around $q \approx -0.6$ for the accelerating η CDM and Λ CDM models. As for the jerk, in Λ CDM, it is strictly unity; in open models, it is less than unity due to the presence of curvature, while for the η CDM model, it has a nontrivial evolution at late times due to the competition between curvature and noise-induced acceleration. First, it grows above 1, then it attains a maximum value of a few, and then it decreases again toward current values slightly larger than unity. This nontrivial behavior of the jerk could be a crucial observable to test the η CDM model in the near future, when data from the Euclid satellite will become available.

Finally, a caveat is in order. We have found that the best-fit values of $\Omega_{m,0}$ in the η CDM model amount to around 0.4, a value appreciably larger than the usual ≈ 0.3 applied for Λ CDM. This will imply that, at a fixed power spectrum normalization (quantified by σ_8 , the mass variance filtered on a scale of $8 h^{-1}$ Mpc), the number density of collapsed halos will be somewhat larger, especially toward high z , an occurrence that may be pleasing in view of recent claims based on early JWST data (e.g., Harikane et al. 2023; Labbé et al. 2023; Xiao et al. 2023). In turn, the larger matter content will produce an enhanced lensing probability, leading to higher CMB lensing, galaxy-CMB lensing cross-correlation, and cosmic shear amplitude. Actually, all of these observables only probe a combination of σ_8 and $\Omega_{m,0}$ to some power (e.g., for cosmic shear, the relevant parameter is $S_8 \equiv \sigma_8 \sqrt{\Omega_{m,0}/0.3}$), so that lowering σ_8 somewhat could still meet the associated observational constraints. Relatedly, in the present work, we focus on the determination of a restricted set of basic cosmological parameters (essentially $\Omega_{m,0}$ and h_0) mainly via Type Ia SNe, BAOs, and the position of the first peak in the

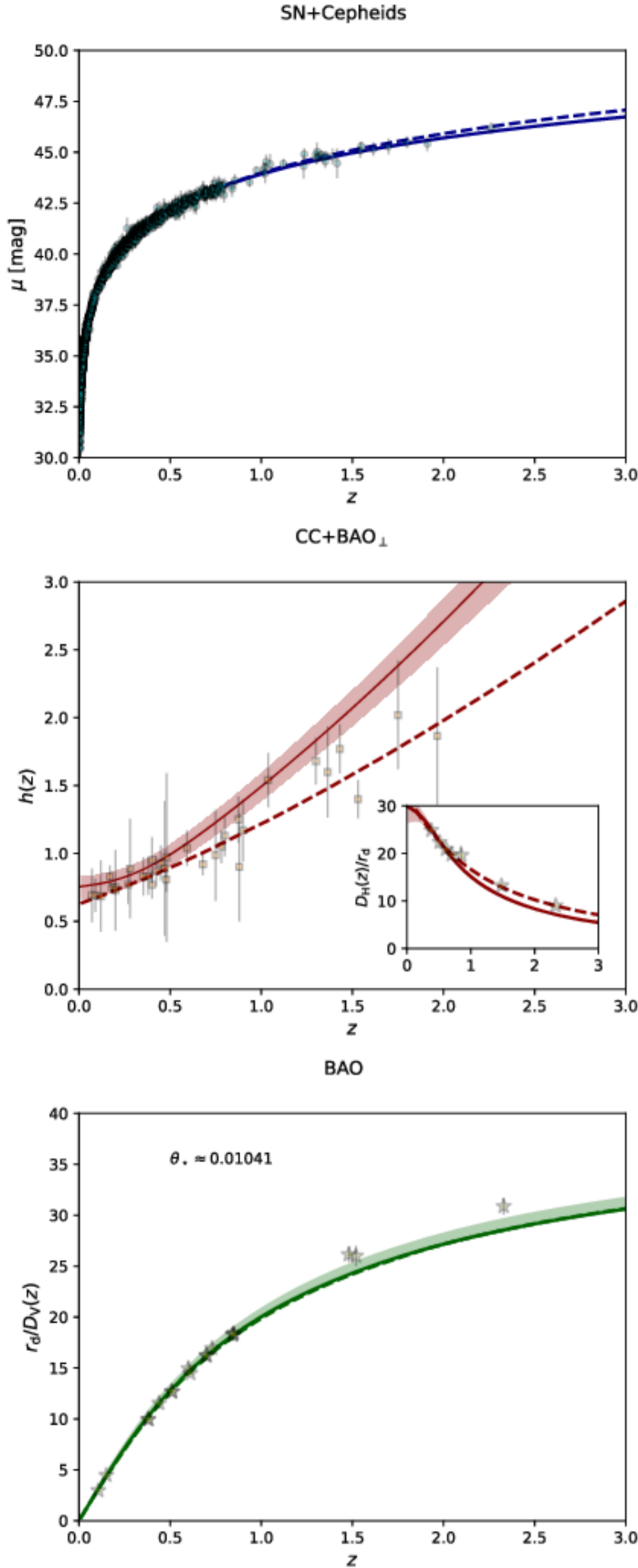


Figure 3. Fits to SN+Cepheid (top panel), CC+BAO $_{\perp}$ (middle panel), and BAO+CMB θ_* (bottom panel) in the r CDM model. In each panel, solid lines and shaded areas illustrate the median and 2σ credible interval from sampling the posterior distribution of the joint analysis, while the dashed line is the median from the posterior distribution of the analysis to the individual data set. Data and references for each observable are described in Section 4.

CMB power spectrum. In the future, it will be necessary to conduct a global analysis of an extended cosmological parameter set (e.g., including primordial spectral index n_s ,

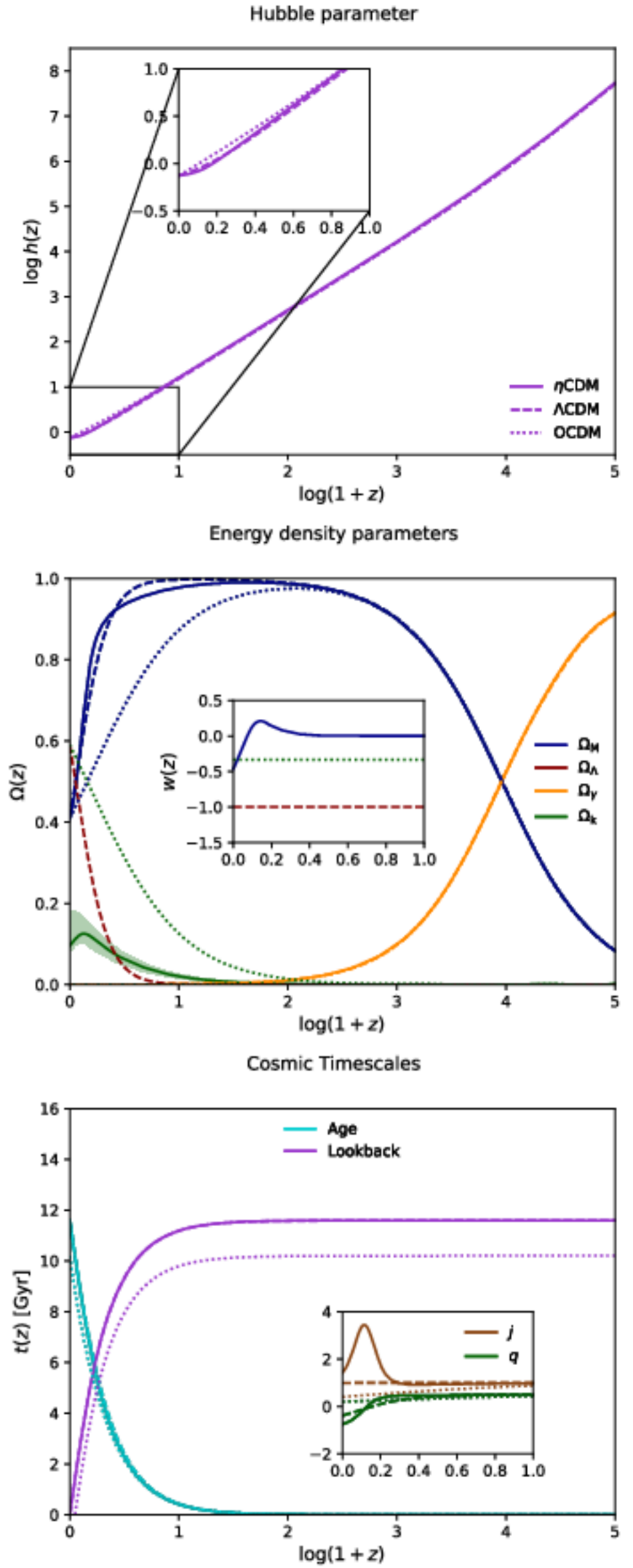


Figure 4. Average evolution in the r CDM model. Top panel: Hubble parameter as a function of redshift; the inset zooms in on the late-time evolution. Middle panel: energy density parameters of matter (blue), dark energy (red), radiation (orange), and curvature (green) as a function of redshift. The inset refers to the equation of state for the dominant energy density component at late times. Bottom panel: age of the Universe (cyan) and look-back time (magenta) as a function of redshift. The inset shows the late-time evolution of the deceleration parameter q (green) and jerk parameter j (brown). In all panels, solid lines are from r CDM with best-fit parameters ($h, \Omega_{m,0}, \zeta, \alpha$) from the joint analysis of Section 4, dashed lines are for a flat Λ CDM with the same parameters ($h, \Omega_{m,0}$), and dotted lines are for an open CDM model with the same parameters ($h, \Omega_{m,0}$). In the middle panel, the green shaded area on the r CDM curvature parameter illustrates the typical 2σ uncertainty on the plotted quantities.

power spectrum normalization σ_8 , etc.) by exploiting the overall CMB power spectra in intensity and polarization and including the aforementioned lensing observables; this could possibly slightly change the best-fit values of $\Omega_{m,0}$ and h_0 derived here.

5. A (Mildly) Stochastic Universe

We now turn to quantifying the random component of the η CDM model. According to the procedure outlined in Appendix B (see Equation (B1)), we need to solve the system of stochastic differential equations (of the Ito type),

$$\begin{cases} \dot{\tilde{h}} = -\frac{\tilde{h}}{\tau_0 - \tau} + \frac{\zeta}{2}(\Omega_m + \Omega_\gamma) h^{\alpha+1} \eta(\tau) \\ \dot{\tilde{\Omega}}_m = -\frac{\tilde{\Omega}_m}{\tau_0 - \tau} + \zeta(1 - \Omega_m - \Omega_\gamma) \Omega_m h^\alpha \eta(\tau) \\ \dot{\tilde{\Omega}}_\gamma = -\frac{\tilde{\Omega}_\gamma}{\tau_0 - \tau} + \zeta(1 - \Omega_m - \Omega_\gamma) \Omega_\gamma h^\alpha \eta(\tau), \end{cases} \quad (12)$$

with initial values $\tilde{h}(\tau_{\text{in}}) = \tilde{\Omega}_m(\tau_{\text{in}}) = \tilde{\Omega}_\gamma(\tau_{\text{in}}) = 0$; we choose τ_{in} corresponding to redshift $z_{\text{in}} \approx 100$, but the results are unaffected as far as $z_{\text{in}} \gtrsim 10$ (i.e., a redshift so large that the noise term of the original process is negligible). In the above equations, recall that, by definition, $h = \bar{h} + \tilde{h}$ and $\Omega_{m,\gamma} = \bar{\Omega}_{m,\gamma} + \tilde{\Omega}_{m,\gamma}$ hold, with the barred quantities constituting the solution for the average behavior found in the previous sections.

We solve the above system with the Euler–Maruyama method⁶ and determine the stochastic evolution of \tilde{h} and $\tilde{\Omega}_{m,\gamma}$ by running 10^4 realizations of the stochastic process. Then we combine such random components with the average ones from Section 3 to reconstruct the overall cosmic history of the Hubble h and energy density parameters $\Omega_{m,\gamma}$ in each patch of the Universe. For an observer measuring the current values of these quantities as estimated in Section 4 by comparison with cosmological observables, the overall evolution is plotted in Figure 5 (in the overall variance, we also include the uncertainties in the determination of h_0 and $\Omega_{m,0}$ from cosmological observables, but this is negligible with respect to that induced by the noise). Specifically, there we illustrate the mean value and the 1σ – 2σ variance induced by the noise as a function of redshift. In the right panels, we also display histograms showing the probability distribution of these quantities at some representative redshifts in the late Universe when noise is appreciably active; these represent the spatial distribution of the cosmological quantities among different patches of the Universe.

The Hubble parameter h fluctuates such that its 1σ variance is about 0.07 dex at $z \approx 0.1$, increases up to 0.13 dex around $z \approx 1$, and then starts to decrease, amounting to 0.08 dex at $z \gtrsim 3$ and becoming progressively negligible at higher redshifts. For Ω_m , the evolution of the variance is faster, being 0.03 dex at $z \approx 0.01$, increasing up to 0.08 dex at $z \approx 0.1$ – 0.3 , and then quickly decreasing to 0.03 dex at $z \approx 1$ and negligible values at higher z ; fluctuations in Ω_κ are similar to these. For Ω_γ , the typical values of the variance are 0.05 dex at $z \approx 0.025$, a maximal 0.1 dex at $z \approx 0.25$, and 0.03 at $z \approx 1$. As already explained, such fluctuations of the relevant cosmological quantities should be interpreted as residual deviations from isotropy/homogeneity on different patches of the Universe. It is a specific prediction of the η CDM model that one should observe the anisotropies/inhomogeneities estimated here via a

⁶ The Euler–Maruyama method is a generalization of the Euler method for stochastic differential equations. It consists of discretizing an Ito-type equation, $\dot{x} = f(x) + g(x)\eta(t)$, as $x(t_{j+1}) = x(t_j) + f(t_j)(t_{j+1} - t_j) + g[x(t_j)]\sqrt{t_{j+1} - t_j} w_j$ in terms of random weights $w_j \in \mathcal{N}(0, \sqrt{2})$ extracted from a normal distribution with zero mean and variance of 2 (e.g., Kloeden & Platen 1992; Risken 1996).

tomographic analysis in redshift shells on different patches of the Universe. Given the magnitude of the fluctuations, such observations will be quite challenging, though possibly within the reach of future wide galaxy surveys like Euclid or LSST.

As anticipated in Section 2, one can now estimate the typical coarse-graining scale associated with the η CDM model. Given that the fluctuation of the overdensity field $\log \Omega \sim \log(1 + \delta)$ induced by the noise amounts to $\lesssim 0.08$ dex, we can exploit the relation between the smoothing scale and variance in the overdensity field from Figure 1 (bottom right panel) and its accuracy of $\lesssim 10\%$ (see Repp & Szapudi 2017, 2018) to estimate an η CDM coarse-graining scale of around $42 \pm 5 h^{-1}$ Mpc. On the one hand, such an estimate must be taken with care, since it has been derived based on N -body simulations performed in Λ CDM; on the other hand, the relation between the smoothing scale and variance in the overdensity field should not vary much given that Λ CDM and η CDM have very similar (spatially averaged) evolution in cosmic time. All in all, we can confidently (at 2σ) quote for η CDM a coarse-graining scale in the range of 30 – $50 h^{-1}$ Mpc. Pleasingly, the coarse-graining scale so obtained corresponds to the typical size of the structures present in the cosmic web, as envisaged in building our stochastic framework in Section 2. Furthermore, on patches of this size, the corresponding fluctuations in matter density $\log \rho \sim \log(\Omega h^2)$ are of order $\lesssim 0.1$ dex, implying in Equation (1) minor deviations from local energy conservation induced by the noise term. Finally, the mean bulk motions on such scales are expected to be $\sim 300 \text{ km s}^{-1}$, which is substantially smaller than the Hubble flow of $\sim 3500 \text{ km s}^{-1}$, thus ensuring that the Friedmann equation can still constitute a safe approximation.

6. The Fate of the Universe

What will be the fate of the Universe in the η CDM model? To answer the question, we go back to Equation (4); in particular, since radiation is negligible at late times (and even more in the future), one can focus on the first two equations for the evolution of \tilde{h} and $\tilde{\Omega}_m$. It is quite easy to realize, and straightforward to confirm numerically, that the system of equations admits an attractor solution in the infinite future; this can be found by putting $\dot{\tilde{h}} = \dot{\tilde{\Omega}}_m = 0$ and solving for the asymptotic values h_∞ and Ω_∞ . A simple algebraic calculation yields

$$\begin{cases} 3\Omega_\infty^2 + 2(4 - \alpha)\Omega_\infty - 4 = 0, \\ h_\infty = \left[\zeta^2 \left(1 - \frac{4 - \alpha}{2} \Omega_\infty \right) \right]^{1/(1 - 2\alpha)}. \end{cases} \quad (13)$$

Therefore, Ω_m tends to a constant, nonzero value that depends solely on the parameter α describing the time dependence of the noise; for the value $\alpha \approx -3/2$, as estimated from the comparison with cosmological data sets in Section 4, one finds $\Omega_\infty \approx 1/3$. Moreover, from Equation (10), it follows that the effective equation of state for matter asymptotes to $w_\infty \approx -1$; as a matter of fact, in the infinite future, matter will behave like a cosmological constant. The limiting value of h also depends on the noise strength ζ , and for the best-fit parameters estimated in Section 4, one finds $h_\infty \approx 0.7$; clearly, from Equation (5), it follows that $q_\infty \approx -1$. This implies that the Universe will continue to expand forever in an exponential way so that the asymptotic behavior of the scale factor $a(t) \propto e^{h_\infty t}$ will apply.

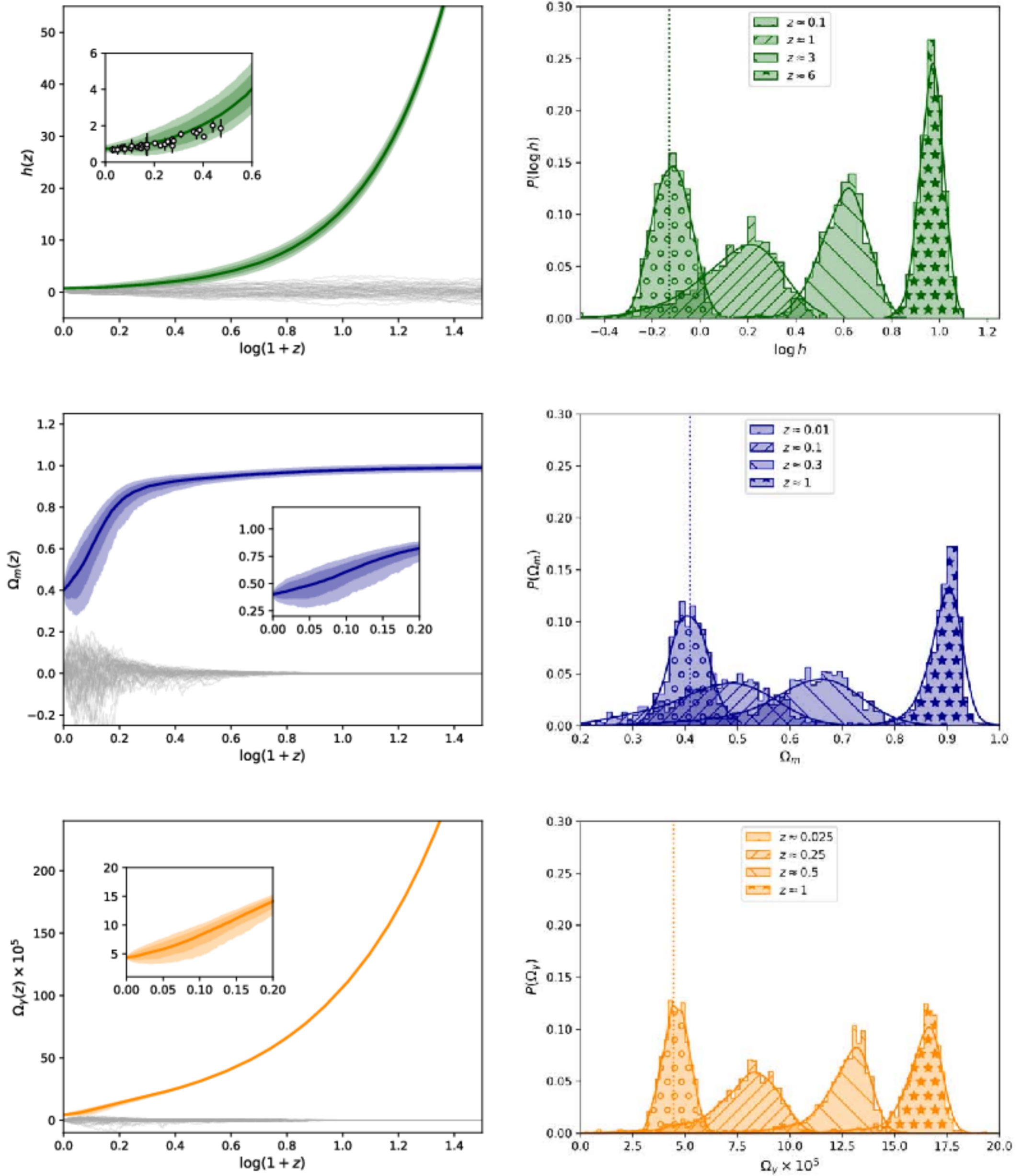


Figure 5. Cosmic evolution and probability distribution of the Hubble (top panels), matter density (middle panel), and radiation density (bottom panel) parameters in the η CDM model. The left panels illustrate the average evolution (colored solid line), the 1σ – 2σ variance of the different quantities as originated by the noise (colored shaded areas), and some examples of the random component departed by the average (gray lines); the insets zoom in on the late-time evolution, with that for $h(z)$ also reporting data from CCs. The right panels illustrate the corresponding probability distributions (histograms and kernel density estimators as solid lines) at different representative redshifts in the late Universe (see legend); the dotted vertical line shows the present value (see Section 4).

Furthermore, Equation (8) directly implies that $\bar{\Omega}_r$ will tend to zero as $\bar{\Omega}_r \propto a^{-3\zeta^2} h_\infty^{2\alpha-1} \Omega_\infty^2/2 \rightarrow 0$ in the infinite future.

A crucial remark is in order here. The current estimates of the parameters $h_0 \approx 0.75$ and $\Omega_{m,0} \approx 0.4$ inferred from comparison with cosmological data sets in Section 4 are very close to the asymptotic values h_∞ and Ω_∞ that will be attained in the infinite future. This occurrence relieves coincidence

problems even in a wide sense; besides waiting for conditions in the Universe that are suitable for the development of life, there is no coincidence at all in the fact that we currently measure certain values of the cosmological parameters h_0 and $\Omega_{m,0}$. This is because the Universe will have values very close to those for essentially an infinite amount of time. In other words, as soon as the noise starts affecting the cosmic evolution

and brings cosmic acceleration into the game, such parameters will stay put or change very little.

This is at variance with the situation in Λ CDM, where in the past, Ω_m was close to 1, Ω_Λ was close to zero, and h was very large, while in the infinite future, Ω_m will tend to zero, Ω_Λ to 1, and h to $\sqrt{\Omega_{\Lambda,0}} h_0$. Given that the currently measured values are in between these extremes (even more, Ω_m and Ω_Λ are of the same order), the coincidence problem is very pressing for Λ CDM; why do we live in this very precise moment of cosmic history? As shown above, the issue is cleared in η CDM.

7. Frequently Asked Questions

Below, we try to answer some questions that may arise in connection with our nonstandard η CDM cosmological model.

1. What about the Meaning of the Noise Term?

The meaning of the noise term is to provide a mean-field description of the slightly different evolution for patches of the Universe that are tens of megaparsecs in size, which are enforced by local inhomogeneities, matter flows due to anisotropic stresses, tidal forces, gravitational torques, and other complex gravitational processes that for all practical purposes are extremely difficult to model ab initio or handle (semi)analytically.

The situation is somewhat analogous to the classic description of Brownian motion. A microscopic particle immersed in a fluid continuously undergoes collisions with the fluid molecules; the resulting motion, despite being deterministic, appears to be random at the macroscopic level, especially to an external observer who has no access to the exact positions and velocities of the innumerable fluid molecules and the initial conditions of the particle. In the way of a statistical macroscopic description, the problem is effectively treated via a stochastic differential equation driven by a fluctuating white noise, which allows one to implicitly account for the complex microscopic dynamics of the system.

Note that the system's state often influences the intensity of the driving noise, like when the Brownian fluctuations of a microscopic particle near a wall are reduced by hydrodynamic interactions, so that the noise becomes multiplicative in terms of a nonuniform diffusion coefficient. This adds complexity to the dynamics because the multiplicative nature of the noise brings a noise-induced drift into the game, which can appreciably affect the overall evolution of the system (even its average component). Similar stochastic models with multiplicative noise have been employed to describe a wide range of physical phenomena, from Brownian motion in inhomogeneous media or close approach to physical barriers, to thermal fluctuations in electronic circuits, to the evolution of stock prices, to computer science, to the heterogeneous response of biological systems and randomness in gene expression (e.g., Risken 1996; Mitzenmacher 2004; Reed & Jorgensen 2004; Paul & Baschnagel 2013). In cosmology, a similar formalism, though with different premises and aims, has also been exploited in models of stochastic inflation (see Vilenkin 1983; Starobinski 1986; Nakao et al. 1988; Salopek & Bond 1990; see also recent review by Cruces 2022 and references therein) and in the field of structure formation to predict the halo mass function and related statistics

(e.g., Bond et al. 1991; Mo & White 1996; Lapi & Danese 2020; Lapi et al. 2022).

In the η CDM model, the noise-induced drift is associated with the multiplicative nature of the stochastic term in the mass–energy evolution equation. As we have shown, it can substantially affect the cosmic dynamics at late times, driving an accelerated expansion, forcing matter to behave as a negative pressure component, and keeping the curvature to small values even in a low-density, matter-dominated Universe.

2. What about the Modeling of the Noise Term?

In the modeling of complex systems (see references above), the stochastic equations and the noise terms are designed on purpose to effectively describe the macroscopic dynamics and then checked by comparison with observations and/or numerical simulations.

In the context of the η CDM model, the noise term can be naively justified by the fact that at a given cosmic time, the overdensity $\log(1 + \delta) \propto \log \rho$ smoothed on a scale of tens of megaparsecs in size is expected to follow a lognormal distribution; as shown in Figure 1, this is proved by simulations to be a good approximation in Λ CDM (see Repp & Szapudi 2018; see also Kayo et al. 2001), and there are theoretical arguments supporting this assumption in general (see discussion by Coles & Jones 1991; see also Neyrinck et al. 2009; Repp & Szapudi 2018). In terms of basic stochastic processes, an ensemble of regions whose density evolves stochastically in time under Gaussian white noise $\eta(t)$ —or, in other words, for which $d \log \rho \sim \dot{\rho}/\rho \propto \eta(t)$ —features as a solution a lognormal distribution with time-dependent variance, as recalled in Appendix A (see also Risken 1996; Paul & Baschnagel 2013). Although the equations ruling the η CDM model (see Equation (1)) describe a more complex stochastic system, this analogy has inspired us to model the noise term as $\dot{\rho} \sim \zeta H^\alpha \rho$, with the parameters ζ and α describing our ignorance of the present value and the redshift evolution of the variance in the density distribution for a generic cosmology that can, in principle, be different from Λ CDM.

The adopted modeling for the noise also avoids adding too much complexity (or too many parameters) and yet satisfies a few physical requirements. First, the stochasticity is driven by Gaussian white noise. In the absence of a detailed control on the gravitational dynamics, this is the natural choice in the modeling of stochastic systems; in future developments, such an assumption can be relaxed by allowing for more complex frameworks with correlated or fractional noise, etc. Second, the linear dependence of the noise on the energy density of cosmic components pleasingly does not break the linear nature of the mass–energy evolution equation. Third, the inverse dependence of the noise term on the Hubble parameter guarantees that the noise term vanishes in the early Universe, where (statistical) isotropy/homogeneity is robustly verified via CMB observations. The choice of a power-law dependence is somewhat arbitrary and has been dictated by our intention of keeping the treatment as simple as possible and limiting the number of noise-related parameters. However, we have checked that the implications for the cosmic dynamics are quite robust against different

parameterizations of this dependence (we tested, e.g., an exponential function of h), though making the equations less transparent. Thus, in this first investigation, we prefer to avoid such complications.

All in all, to describe the phenomenon of cosmic acceleration, the η CDM model features the same number of parameters as the standard Λ CDM cosmology. In Λ CDM, an additional component is added with abundance $\Omega_{\Lambda,0}$ and equation of state w_{Λ} (whose evolution, in turn, can be characterized by one or more parameters). In η CDM, no additional component is added, and two parameters are needed to describe the strength and redshift dependence of the noise; the ensuing evolution of the cosmic dynamics at late times is completely specified (also including an effective, time-dependent equation of state for the matter component; see Equation (10)).

3. What about Alternative Physical Interpretations of Stochasticity on Large Scales?

In the literature, other origins for stochasticity on cosmological scales, though rather different from our viewpoint, have been envisaged; for the sake of completeness, we briefly mention them below.

Stochasticity can be plausibly created by baryonic physics ongoing in collapsed objects (e.g., galaxies or clusters), such as turbulence, feedback processes from SN explosions or AGN outbursts/jets, etc. The problem with this scenario is that such effects are rather contained in space, influencing patches from kiloparsec to at most megaparsec scales. In fact, it has been argued that the effective casual limit of a galaxy is set by scales attained by matter flows around it over the age of the Universe, rather than by its usual light cone (see Ellis & Stoeger 2009). However, there are some proposed mechanisms to transfer such randomness on much larger cosmological scales via chaotic dynamics or spontaneous stochasticity (a kind of “butterfly effect”), but definite conclusions on their effectiveness are still far from being drawn (see Neyrinck et al. 2022 and references therein).

Stochasticity is also naturally created at the quantum level. In this vein, a spatially fluctuating field that describes random matter/radiation creation or disappearance could permeate the Universe (e.g., Sivakumar et al. 2001; Lima et al. 2008; Amin & Baumann 2016; Mantinan et al. 2023). Albeit being highly exotic, the problem with such a scenario is that it requires some unspecified mechanism (a sort of quantum spontaneous stochasticity; see Eyink & Drivas 2015) to allow such tiny fluctuations to expand, reinforce, and become large enough to ultimately influence astrophysical and cosmological scales; moreover, a specific coupling of such a random field with the gravitational metric is possibly required to affect the cosmic dynamics at late times.

4. Is the η CDM Model Violating the Cosmological or Copernican Principles?

The cosmological principle is violated, but with a grain of salt. The η CDM model does not suggest strong violation of isotropy or homogeneity on horizon scales, which would require us to completely change our view of the Universe and the description of the gravitational metric (e.g., reverting to a Lematre–Tolman–Bondi or Swiss-cheese universe; e.g., see Marra et al. 2007).

Instead, it just advocates, as supported by numerical simulations (see Section 2), that small deviations of isotropy/homogeneity are present on scales of tens of megaparsecs associated with the quasi-linear structures of the cosmic web.

The Copernican principle is not violated, either in the strict (humans on Earth are not privileged observers) or in the enlarged (no one in the Universe is a privileged observer) sense. In the η CDM, violation of isotropy and homogeneity are small and imply minor fluctuations of the cosmological quantities on top of a still dominant yet noise-informed average evolution. Every observer in the Universe will measure similar values of the cosmological parameters and should be able to statistically verify the same small deviations from isotropy/inhomogeneities on large scales.

5. What Is the Origin of the Cosmic Acceleration in η CDM?

In η CDM, the cosmic acceleration is caused by the noise-induced drift appearing in Equation (4), which represents the ensemble-averaged evolution of the stochastic system described by Equation (3). It is instructive to mathematically and physically understand how the cosmic acceleration comes about from a heuristic analysis of the original Friedmann, mass–energy evolution, and acceleration equations (see Equations (1) and (2)). This can be done by considering the following argument based on simple scaling laws. Neglecting curvature from the Friedmann equation $H \sim \rho^{1/2}$ applies; hence, the random term in the mass–energy evolution equation scales as $\dot{\rho} \sim \zeta \rho H^{\alpha} \eta \sim \zeta \rho^{1+\alpha/2} \eta$, while that in the acceleration equation goes like $\ddot{a} \sim \zeta \rho H^{\alpha-1} \eta \sim \zeta \rho^{(1+\alpha)/2} \eta$; given that $\alpha \sim -1.5$, the scaling exponent $1 + \alpha/2 > 0$ in the equation for $\dot{\rho}$ is positive, while $(1 + \alpha)/2 < 0$ in the equation for \ddot{a} is negative.

This implies that a fluctuation induced by the noise η will be reinforced in high-density regions (e.g., filaments, knots) as for the variation of ρ , but at the same time, it will be softened in terms of contribution to the acceleration; contrariwise, in low-density regions (voids), the fluctuation will be damped in terms of $\dot{\rho}$, while it will be amplified in terms of \ddot{a} . All in all, this mechanism would statistically cause the overall ensemble of patches to drift toward an evolution dominated by low-density regions and characterized by an enhanced expansion rate.

6. Is η CDM a Backreaction Model?

Our stochastic cosmology is inspired and has some features in common with Newtonian backreaction models, so it is worth pointing out the similarities and crucial differences between these frameworks.

Newtonian (also called kinematical) backreaction is a class of models that originated in a seminal paper by Buchert & Ehlers (1997), who explored the effects of matter anisotropy/inhomogeneities on the expansion rate of a given patch of the Universe. Specifically, the authors performed spatial averaging on an arbitrary domain of volume V to derive an equation for the evolution of the local expansion factor $a \equiv V^{1/3}$; working in a Newtonian framework and assuming mass conservation and a pressureless matter component, they got the modified

acceleration equation

$$\frac{\ddot{a}}{a} = -\frac{4\pi G}{3}\langle\rho_m\rangle + \frac{2}{9}(\langle\dot{a}^2\rangle - \langle\dot{a}\rangle^2) + \frac{2}{3}\langle\omega^2 - \sigma^2\rangle, \quad (14)$$

where $\langle\rho_m\rangle$ is the average density in the volume, and ω and σ are the magnitude of the rotation and shear tensors. The terms on the right-hand side account for the fact that anisotropy/inhomogeneities in the matter distribution can modify the average expansion rate of the volume, which for particular conditions could also be driven to accelerate (e.g., Kolb 2011; Buchert & Räsänen 2012). However, backreaction effects depend on the size of the volume under consideration, and it is generally assumed that these rapidly decrease for scales larger than the largest inhomogeneity (see Kaiser 2017); on the other hand, this treatment neglects the possibly different evolutions of the various patches because of the local inhomogeneities/anisotropies, matter flows, and the overall consequence of sampling effects on the cosmic dynamics.

The η CDM framework shares with the above backreaction models the general idea that structure formation could possibly modify the expansion rate on larger scales. However, it attacks the problem with a different statistical approach that envisages the Universe tessellated with patches of tens of megaparsecs in size where residual anisotropy/inhomogeneity, as indicated by numerical simulations, is still present. Such regions will undergo slightly different evolutions due to local inhomogeneities, matter flows, and many complex gravitational processes. The detailed dynamics is extremely difficult to follow (semi)analytically; hence, a statistical description of the evolution of the different patches is adopted in terms of a stochastic noise term in Equation (2), whereas the global evolution of the Universe is then derived by averaging the behavior over the patch ensemble.

In this respect, our approach is reminiscent of the Average Expansion Rate Approximation (AvERA) algorithm (see Racz et al. 2017); this is a procedure to extract the cosmological expansion rate from an N -body simulation via a volume-averaging technique. The basic idea of AvERA is to account for local inhomogeneities by inverting the usual order of volume-averaging and expansion rate computation in the simulation; first, small patches of the Universe with a certain coarse-graining scale are evolved via the standard Friedmann equation (with no dark energy) according to the local density, and then the global expansion rate is obtained by volume-averaging over the local scale factor increments. Remarkably, the net outcome is a global expansion history mirroring that of the standard Λ CDM model.

In AvERA and the η CDM model, the cosmic acceleration originates from the same basic underlying physics, i.e., that the nature of the large-scale structure formation places far more volume in underdense than overdense regions, causing the average expansion to skew toward acceleration. Both in AvERA and in the η CDM model, the coarse-graining scale involved is essentially a free parameter (a spatial smoothing scale used in the simulation for AvERA and a quantity fully specified by the noise parameters ζ and α for the η CDM model) that is set by comparison with data.

However, in AvERA, the coarse-graining scale is

found to be smaller than a few megaparsecs (which corresponds to $\lesssim 10^{12} M_\odot$), while in the η CDM model, it turns out to be several tens of megaparsecs (which are associated with the quasi-linear structures of the cosmic web). This difference in the effective coarse-graining scale can be traced back to the diverse assumptions of the two models. Specifically, the AvERA approach is rooted in the separate Universe conjecture, meaning that spherically symmetric patches of the Universe are assumed to behave like isolated islands evolving with their own energy density $\Omega \sim 1 + \delta$, while anisotropic stresses, tidal forces, external environment, and cross talk of different regions by flows of matter and radiation are neglected (see also Buchert 2018). On the other hand, the η CDM model allows for such processes to occur, admittedly at the price of reverting to a mean-field statistical description in terms of a phenomenological yet physically reasonable noise term.

To sum up, AvERA and the η CDM constitute somewhat complementary approaches, concurring to suggest that structure formation on nonlinear and quasi-linear spatial scales can have relevant effects on the overall cosmic expansion.

8. Summary

We have proposed a new model of the Universe called η CDM. Its marking feature is a controlled stochastic evolution of the cosmological quantities that is meant to render the effects of small deviations from homogeneity/isotropy on large scales of tens of megaparsecs in size at late cosmic times associated with the emergence of the cosmic web. Specifically, we prescribe that, still in the context of standard general relativity, the evolution of the matter/radiation energy densities in different patches of the Universe can be effectively described by a stochastic version of the mass–energy evolution equation. The latter includes, besides the usual dilution due to cosmic expansion, an appropriate multiplicative and time-dependent noise term that statistically accounts for local fluctuations due to inhomogeneities and matter flows induced by anisotropic stresses and many complex gravitational processes. The different evolution of the patches as a function of cosmic time is rendered via the diverse realizations of the noise term; meanwhile, at any given cosmic time, sampling the ensemble of patches will create a nontrivial spatial distribution of the various cosmological quantities. Finally, the overall behavior of the Universe will be obtained by averaging over the patch ensemble. We have assumed a very simple and physically reasonable parameterization of the noise term, gauging it against a wealth of cosmological data sets in the local and high-redshift Universe, including SN+Cepheid cosmography, baryon acoustic oscillations, cosmic chronometers, CMB first angular peak position, and age estimates from globular clusters.

We have found that, with respect to standard Λ CDM, the cosmic dynamics in the η CDM model is substantially altered by the noise in three main respects. First, an accelerated expansion is enforced at late cosmic times without the need for any additional exotic component (e.g., dark energy); the physical interpretation of this effect is that the overall ensemble of patches tends to drift toward an evolution dominated by low-density regions. Second, the global spatial curvature can stay small even in a low-density Universe constituted solely by

matter and radiation. Third, matter can acquire an effective negative pressure at late times. We have also pointed out that the η CDM model is Hubble tension-free, meaning that the estimates of the Hubble constant from early- and late-time measurements do not show marked disagreement as in Λ CDM. We have then provided specific predictions for the variance of the cosmological quantities induced by the noise at late cosmic times, which is found to be associated with the residual deviation from homogeneity/isotropy on large scales of order tens of megaparsecs. These could be tested with observations covering wide areas and large redshift intervals via a tomographic analysis; such observations could be quite challenging but within the reach of future surveys like Euclid or LSST.

Remarkably, the η CDM model admits an attractor solution in the infinite future with very peculiar features; the Universe will expand exponentially, $a \propto e^{h_\infty t}$, with an e-folding time given by a limiting value of the Hubble parameter h_∞ ; the matter energy density parameter will saturate to a constant non-null value Ω_∞ and will be characterized by an effective equation of state $w_\infty \approx -1$, i.e., it will behave like a cosmological constant; and the curvature will go to zero. Remarkably, the limiting values h_∞ and Ω_∞ are found to be only slightly smaller than the present ones; this implies that the Universe will spend a very long (actually, infinite) amount of time hovering around very similar values of the cosmological parameters, thus resolving any cosmic coincidence issue even in a wide sense without strongly invoking anthropic considerations.

In a future perspective, it would be welcome to explore whether different types of noise (e.g., beyond the white-noise approximation) can alter the cosmic dynamics; investigate whether the small residual anisotropy/inhomogeneity on large scales can appreciably perturb the gravitational metric and estimate how the related corrections can impact the estimation of the noise and cosmological parameters; study the evolution of perturbations and gauge the model parameters via an extended analysis of the overall CMB power spectrum, the integrated Sachs & Wolfe effect, and CMB lensing; compute the growth function for cosmic structure formation and the effects on weak lensing probes and hopefully address the S_8 tension; and provide specific predictions for the observability of the implied anisotropies/inhomogeneities in future surveys both via standard messengers and via gravitational waves.

We conclude with disclaiming that the η CDM framework presented here is just a very basic model, and that substantial work will admittedly be required for elevating it to a self-contained cosmology and fully testing it against next-generation data sets. However, we very much hope that the new perspectives offered by the η CDM framework will contribute to triggering further attempts at explaining the observed phenomenology in the late-time cosmic expansion and curing the plagues in the standard cosmological model, not necessarily invoking exotic forms of energies or substantially revisiting the standard (and, up to now, observationally undefeated) Einstein theory of gravity.

Acknowledgments

We thank the referee for a constructive report and the very useful suggestions on how to substantially improve the presentation of our work. We acknowledge A. Bressan, G. Gandolfi, C. Ranucci, and the GOTHa team at SISSA for

illuminating comments. A.L. dedicates the present work to M. Massardi, who has supported him in this great endeavor and tolerated long (and likely annoying to a radio astronomer like her) discussions on the subject. This work is funded by the PRIN MIUR 2017 prot. 20173ML3WW, “Opening the ALMA window on the cosmic evolution of gas, stars and supermassive black holes”; the EU H2020-MSCA-ITN-2019 Project 860744 “BiD4BEST: Big Data applications for black hole Evolution STudies”; the Fondazione ICSC—Spoke 3 Astrophysics and Cosmos Observations—National Recovery and Resilience Plan Project ID CN-00000013 “Italian Research Center on High-Performance Computing, Big Data and Quantum Computing” - Next Generation EU; the project “Data Science methods for MultiMessenger Astrophysics & Multi-Survey Cosmology” funded by the Italian Ministry of University and Research, Programmazione triennale 2021/2023 (DM n.2503 dd. 09/12/2019), Programma Congiunto Scuole; and the INAF Large Grant 2022 funding scheme with the project “MeerKAT and LOFAR Team up: a Unique Radio Window on Galaxy/AGN co-Evolution.”

Appendix A Stochastic Differential Equations

In this Appendix, we provide a primer on stochastic differential equations, pointing out the mathematical meaning of the noise term, the implications of adopting different stochastic prescriptions (e.g., Ito versus Stratonovich), and the related origin of noise-induced drift terms; for more details and mathematical proofs, the reader may have a look at the classic textbooks by Risken (1996) and Paul & Baschnagel (2013).

Consider an n -dimensional variable $\mathbf{x} = \{x_i; i = 1 \dots n\}$ satisfying the stochastic differential equation

$$\dot{x}_i = f_i(\mathbf{x}) + g_{ij}(\mathbf{x})\eta_j(t), \quad (\text{A1})$$

where $\{f_i; i = 1 \dots n\}$ is called the drift vector, $\{g_{ij}; i = 1 \dots n, j = 1 \dots m\}$ is called the diffusion matrix, and $\{\eta_j; j = 1 \dots m\}$ is a vector of independent noise with properties $\langle \eta_i(\tau) \rangle = 0$ and $\langle \eta_i(\tau)\eta_j(\tau') \rangle = 2\delta_{ij}\delta(\tau - \tau')$; bold characters indicate vectors, and summation over repeated indices is implicitly understood.

The mathematical meaning of the noise term $\eta_i(t)$ in the stochastic differential equation can be clarified as follows. For the sake of simplicity, the reader may focus on the one-dimensional case, i.e., the scalar equation $\dot{x} = f(x) + g(x)\eta(t)$, and consider that x refers to some physical property; e.g., with reference to the main text, it could be the density ρ associated with a given patch of the Universe. At every time t , the noise $\eta(t)$ should be considered as a value randomly extracted from a Gaussian distribution with zero mean and variance 2 (by the conventional correlation property of the noise; but actually, this can be put to any value by appropriately redefining g). For any realization of the noise, the variable $x(t)$ will execute a random walk, as schematically depicted in Figure A1; e.g., in the main text, this can represent the specific evolution of the density in a given patch of the Universe. A different realization of the noise will yield a different walk, and so on and so forth. At any given time $t = T$, sampling the value of the variable x from the ensemble of walkers would yield a nontrivial probability distribution $\mathcal{P}(x, T)$ of the variable x , which is the solution to the stochastic differential equation; e.g., in the main text, this distribution

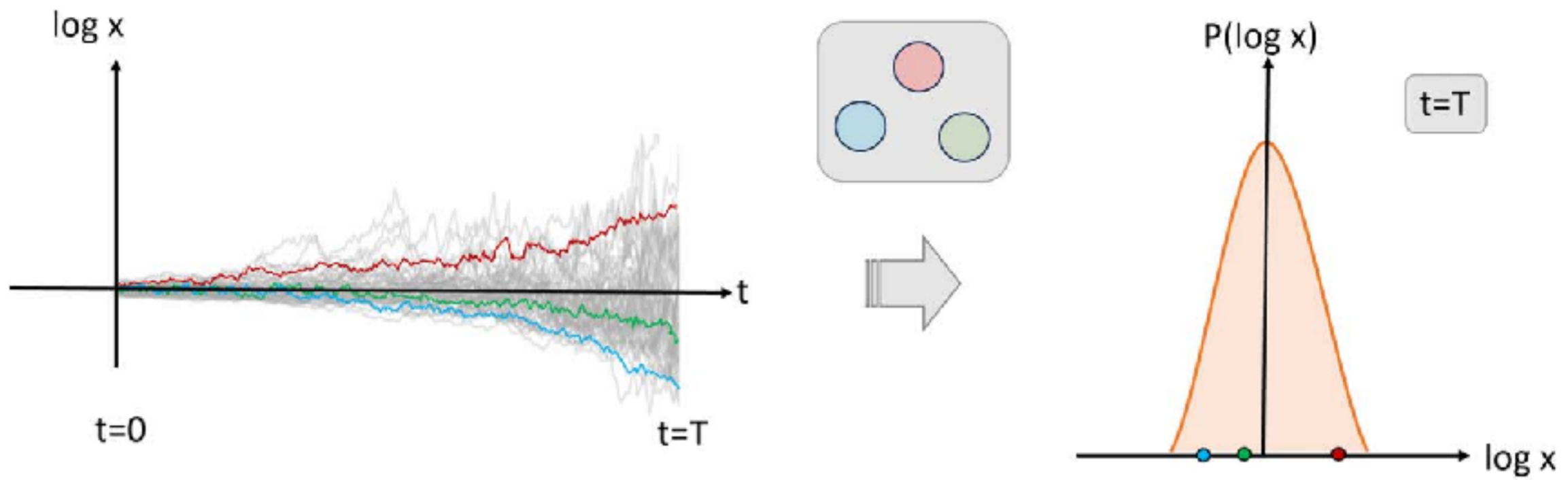


Figure A1. Schematics that illustrate the mathematical meaning of a stochastic differential equation $\dot{x} = f(x) + g(x)\eta(t)$. Each realization of the noise $\eta(t)$ yields a different random walk (e.g., with reference to the main text, the walkers in red, blue, and green correspond to the evolution of the density in three regions at different spatial locations). At a given time $t = T$, sampling the value of the variable x from the ensemble of walkers (e.g., from the different patches in the Universe) would yield a nontrivial probability distribution $P(x, T)$ of the variable x , which is the solution to the stochastic differential equation. The average \bar{x} of this distribution will evolve in time as prescribed by Equation (A5).

represents the spatial distribution of the density in different patches of the Universe.

Generally, solving a stochastic differential equation and obtaining the distribution $\mathcal{P}(x, T)$ requires a numerical approach (e.g., see textbook by Kloeden & Platen 1992). Nevertheless, it is worth mentioning a few very basic examples with constant drift and diffusion coefficients and initial condition $x(0) = x_{\text{in}}$, which admit a closed-form analytic solution. One is the Brownian motion, which describes a basic fluctuating process defined by the equation $\dot{x} = \mu + \sigma \eta(t)$; the solution is a normal distribution $\mathcal{P}(x, T) = \mathcal{N}(\bar{x}, \sigma_x)$ with mean $\bar{x} = x_{\text{in}} + \mu T$ and variance $\sigma_x^2 = \sigma^2 T$. Another is the Ornstein–Uhlenbeck model, which is defined by $\dot{x} = \kappa(\mu - x) + \sigma \eta(t)$ and describes a process naturally falling back to an equilibrium level; the solution is a normal distribution $\mathcal{P}(x, T) = \mathcal{N}(\bar{x}, \sigma_x)$ with mean $\bar{x} = \mu - (\mu - x_{\text{in}})e^{-\kappa T}$ and variance $\sigma_x^2 = (\sigma^2/2\kappa)(1 - e^{-2\kappa T})$. Yet another is the geometric Brownian motion, which is defined by $\dot{x} = \mu x(t) + \sigma x(t)\eta(t)$ and often exploited in finance to model stock prices; the solution is a lognormal distribution $\mathcal{P}(x, T) = \text{LogN}(\bar{x}, \sigma_x^2)$ with average $\bar{x} = x_{\text{in}} e^{\mu T}$ and variance $\sigma_x^2 = x_{\text{in}}^2 e^{2\mu T}(e^{\sigma^2 T} - 1)$.

In the general case of Equation (A1), the stochastic equations are vectorial, and the drift/diffusion coefficients are a nontrivial function of x ; hence, things get very complicated. When naively trying to solve the equations by integrating both sides in time, a well-known problem arises: the delta-correlated nature of the noise requires one to give a meaning to the ill-defined integral

$$\int dt g_{ij}[\mathbf{x}(t)] \eta_j(t) = \lim_{n \rightarrow \infty} \sum_{\ell=1}^n g_{ij}[\mathbf{x}(\tau_\ell)] [\eta_j(t_{\ell+1}) - \eta_j(t_\ell)]. \quad (\text{A2})$$

Note that here, since the variables are stochastic, the limit is meant in the mean-square sense; i.e., $\lim_{n \rightarrow \infty} X_n = X$ stands for $\lim_{n \rightarrow \infty} \langle (X_n - X)^2 \rangle = 0$, where $\langle \cdot \rangle$ denotes an average over the ensemble. For a smooth function, the limit converges to a unique value independent of τ_ℓ , but this is not the case for the white noise η , since it fluctuates an infinite number of times with infinite variance in any small time interval (it is nowhere differentiable). Thus, the result depends on the choice of τ_ℓ in

the expression $g_{ij}[\mathbf{x}(\tau_\ell)] = g_{ij}[(1 - \omega)\mathbf{x}(t_\ell) + \omega\mathbf{x}(t_{\ell+1})]$, with $\omega \in [0, 1]$. Different choices of ω imply different rules for stochastic calculus; for example, for an arbitrary function $F[\mathbf{x}(t)]$ of the stochastic variables, one can demonstrate that

$$d_t F[\mathbf{x}(t)] = \partial_i F[\mathbf{x}(t)] \dot{x}_i + (1 - 2\omega) g_{ik}(\mathbf{x}) g_{jk}(\mathbf{x}) \partial_i \partial_j F[\mathbf{x}(t)] \quad (\text{A3})$$

holds. Two common choices are the midpoint Stratonovich prescription ($\omega = 1/2$) and the Ito prepoint prescription ($\omega = 0$); the former is mostly used by physicists and the latter by mathematicians and numerical analysts. Note that the choice of the prescription is made on the basis of convenience, since, plainly, the overall dynamics of the system must be unique; in fact, it is possible to represent the same stochastic process in two arbitrary different prescriptions $\omega_1 \rightarrow \omega_2$ just by appropriately rescaling the drift vector (e.g., Moreno et al. 2019),

$$f_i(\mathbf{x}) \rightarrow f_i(\mathbf{x}) + 2(\omega_1 - \omega_2) g_{kj}(\mathbf{x}) \partial_k g_{ij}(\mathbf{x}). \quad (\text{A4})$$

In the main text, we adopt the Stratonovich prescription ($\omega = 1/2$), since it has the advantage that, as shown by Equation (A3), the standard rules of calculus continue to hold, and this makes it easier to analytically manipulate the stochastic equations. However, this comes at a price; the average evolution $\bar{x}(t)$ of the stochastic process in Equation (A1) is ruled by the equation

$$\dot{\bar{x}}_i = f_i(\bar{\mathbf{x}}) + g_{kj}(\bar{\mathbf{x}}) \partial_k g_{ij}(\bar{\mathbf{x}}) \quad (\text{A5})$$

and hence depends not only on the true drift f_i (as is true for the Ito prescription) but also on an additional noise-induced term (see Equation (A4)) that needs to be calculated. Demonstrating the above equation requires one to evaluate the Kramers–Moyal coefficient and derive the Fokker–Planck equation associated with the stochastic differential equations; a primer palatable for astrophysicists and cosmologists can be found in Appendix A of Lapi & Danese (2020) and the classic textbook by Risken (1996). However, naively, the nature of the noise-induced drift can be understood by looking at the basic scalar equation $\dot{x} = f(x) + g(x)\eta(t)$. Taking the average on both sides yields $\dot{\bar{x}} = \langle f(x) \rangle + \langle g(x)\eta(t) \rangle$. Clearly, $\langle f(x) \rangle = f(\bar{x})$ holds, since $f(x)$ is a purely deterministic function of x . The

other term is less trivial, although at first sight, one may think it is null, since $\langle \eta(t) \rangle = 0$ holds by the property of the white noise. However, this is not true, since as $\eta(t)$ varies, $x(t)$ and hence $g(x(t))$ also change, making $\langle g(x)\eta(t) \rangle$ finite; it is this instance that eventually leads to the noise-induced drift.

To make contact with the main text, note that the fundamental Equation (3) constitutes a particular case of Equation (A1) for the three cosmological variables $\mathbf{x} \equiv (h, \Omega_m, \Omega_\gamma)$ when just an independent noise η is present. Specifically, one can define the following components: for the variable vector, $x_0 = h$, $x_1 = \Omega_m$, and $x_2 = \Omega_\gamma$; for the drift vector, $f_0 = h^2(-1 - \Omega_m/2 - \Omega_\gamma)$, $f_1 = \Omega_m h(-1 + \Omega_m + 2\Omega_\gamma)$, and $f_2 = \Omega_\gamma h(-2 + \Omega_m + 2\Omega_\gamma)$; for the noise vector, $\eta_0 = \eta$ and $\eta_1 = \eta_2 = 0$; and for the diffusion matrix, $g_{00} = \zeta/2 (\Omega_m + \Omega_\gamma) h^{\alpha+1}$, $g_{10} = \zeta(1 - \Omega_m - \Omega_\gamma) \Omega_m h^\alpha$, and $g_{20} = \zeta(1 - \Omega_m - \Omega_\gamma) \Omega_\gamma h^\alpha$, with all other components null. Then it is simple algebra to verify that Equation (3) can be put in the vectorial form expressed by Equation (A1).

For the system of Equation (3), computing the noise-induced drift and so obtaining the average evolution described by Equation (4) is straightforward but quite tedious. For the reader's convenience, we report some details of the computation for the component $x_0 = h$; considering only the non-null elements in the summation involved in Equation (A5), one has $\dot{x}_0 = f_0(\bar{x}) + g_{00}(\bar{x}) \partial_{x_0} g_{00}(\bar{x}) + g_{10}(\bar{x}) \partial_{x_1} g_{00}(\bar{x}) + g_{20}(\bar{x}) \partial_{x_2} g_{00}(\bar{x})$, or, in more explicit form, $\dot{h} = \bar{h}^2(-1 - \bar{\Omega}_m/2 - \bar{\Omega}_\gamma) + (\zeta^2/2) \bar{\Omega}_m (1 - \bar{\Omega}_m - \bar{\Omega}_\gamma) \bar{h}^{2\alpha+1} + (\zeta^2/2) \bar{\Omega}_\gamma (1 - \bar{\Omega}_m - \bar{\Omega}_\gamma) \bar{h}^{2\alpha+1} + (\zeta^2/4)(\alpha + 1)(\bar{\Omega}_m + \bar{\Omega}_\gamma)^2 \bar{h}^{2\alpha+1}$. Simplifying the last three addenda, one finally obtains $\dot{h} = \bar{h}^2(-1 - \bar{\Omega}_m/2 - \bar{\Omega}_\gamma) + (\zeta^2/2)(\bar{\Omega}_m + \bar{\Omega}_\gamma)[1 - (1 - \alpha)(\bar{\Omega}_m + \bar{\Omega}_\gamma)/2] \bar{h}^{2\alpha+1}$, which is the first of Equations (4); this explicitly includes on the right-hand side both the true and noise-induced drifts. The average evolution equations for Ω_m and Ω_γ can be derived analogously.

Appendix B Diffusion Bridges

In this Appendix, we provide some basic information on diffusion bridges, i.e., stochastic processes pinned at both ends in some values. For more details, the reader may consult the papers by Pedersen (1995), Durham & Gallant (2002), Delyon & Hu (2006), Lindstrom (2012), Bladt & Sørensen (2014), Whitaker et al. (2017), and Heng et al. (2022).

Suppose one has an N -dimensional continuous stochastic process $\mathbf{x}(t) = \{x_i; i = 1 \dots N\}$ for $t \in [0, T]$ satisfying the system $\dot{x}_i(t) = f_i(\mathbf{x}, t) + g_{ij}(\mathbf{x}, t) \eta_j(t)$ in the Stratonovich sense, with a boundary value $\mathbf{x}(T) = \mathbf{x}_T$ and the property that the random term becomes negligible at early times. Here $\{f_i; i = 1 \dots N\}$ is a drift vector, $\{g_{ij}; i, j = 1 \dots N\}$ is a diffusion matrix, and $\{\eta_j; j = 1 \dots N\}$ is a vector of independent noises; repeated summation convention is adopted.

To (approximately) solve the stochastic system, the idea is to partition the process $\mathbf{x} = \bar{\mathbf{x}} + \tilde{\mathbf{x}}$ in an average $\bar{\mathbf{x}}$ and a residual random $\tilde{\mathbf{x}}$ component, satisfying the system of coupled equations:

$$\begin{cases} \dot{\bar{x}}_i(t) = f_i(\bar{\mathbf{x}}) + g_{kj}(\bar{\mathbf{x}}) \partial_k g_{ij}(\bar{\mathbf{x}}), & \bar{\mathbf{x}}(T) = \mathbf{x}_T \\ \dot{\tilde{x}}_i(t) = -\frac{\tilde{x}_i(t)}{T-t} + g_{ij}(\mathbf{x}) \eta_j(t), & \tilde{\mathbf{x}}(0) = 0. \end{cases} \quad (\text{B1})$$

The first equation describes the average evolution of the system and is analogous to Equation (A5); the first term on the right-

hand side is the true drift, while the second term is the noise-induced one. Being an ordinary differential equation, this can be evolved backward to the initial time via standard methods to provide an initial condition $\mathbf{x}(0) = \mathbf{x}_0$ for the full system.

The second equation is less trivial; it describes a residual random process (in the Ito sense), executing a conditioned diffusion that starts in $\tilde{\mathbf{x}}(0) = 0$ by the boundary condition, and is also forced to end in $\tilde{\mathbf{x}}(T) = 0$ by the spurious drift term $-\tilde{x}_i/(T-t)$ in such a way that the overall stochastic process $\mathbf{x} = \bar{\mathbf{x}} + \tilde{\mathbf{x}}$ behaves as expected, with $\mathbf{x}(0) = \mathbf{x}_0$ and $\mathbf{x}(T) = \mathbf{x}_T$ at the extremes. The origin of the spurious drift is a bit technical. In fact, it can be rigorously demonstrated (e.g., Rogers & Williams 2000) that a diffusion process $\dot{x}_i(t) = g_{ij}(\mathbf{x}, t) \eta_j(t)$ with null drift constrained to start and end in zero (in the Ito convention) is equivalent to an unconditioned process with a spurious drift that forces the walker to hit the final condition of the form $\dot{x}_i(t) = g_{ik}(\mathbf{x}, t) g_{kj}(\mathbf{x}, t) \nabla_j \mathcal{P}(0, T|\mathbf{x}, t) + g_{ij}(\mathbf{x}, t) \eta_j(t)$, where \mathcal{P} is the transition density of the unconditioned process. Since \mathcal{P} is untractable in most cases, a linear Gaussian approximation to it is often adopted (the so-called modified diffusion bridge; see Durham & Gallant 2002; Delyon & Hu 2006) that leads to the spurious drift reported in the second of Equations (B1). Involving an ordinary and a stochastic differential equation, the above system can be solved forward in time via standard numerical techniques, with the only caveat that the argument of the diffusion matrix on the right-hand side of the second equation is the full process $\mathbf{x} = \bar{\mathbf{x}} + \tilde{\mathbf{x}}$; hence, the second equation requires the solution of the first as an input.

In the main text, all of the above has been applied to the original stochastic system in Equation (3) to obtain Equation (4) for the average evolution exploited in Section 3 (see derivation in Appendix A) and Equation (12) for the random part exploited in Section 5. For example, to derive the latter, consider the zeroth component of the second of Equations (B1) that reads $\dot{\tilde{x}}_0(t) = -\tilde{x}_0(t)/(T-t) + g_{00}(\mathbf{x}) \eta(t)$. Recalling from Appendix A that $\mathbf{x} \equiv (h, \Omega_m, \Omega_\gamma)$ and that $g_{00} = (\zeta/2)(\Omega_m + \Omega_\gamma) h^{\alpha+1}$ in terms of the cosmological variables, we obtain $\dot{\tilde{h}}(t) = -\tilde{h}/(T-t) + (\zeta/2)(\Omega_m + \Omega_\gamma) h^{\alpha+1} \eta(t)$, which is the first of Equations (12). The equations for the other components corresponding to Ω_m and Ω_γ are derived analogously.

Appendix C Validation of the Fitting Pipeline

In this Appendix, we validate our fitting pipeline described in Section 4 by applying it to the (curvature-free) Λ CDM model. To this purpose, we solve the evolution equations

$$\begin{cases} \dot{h} = h^2 \left(-1 - \frac{\Omega_m}{2} - \Omega_\gamma - \Omega_\Lambda \frac{1+3w_\Lambda}{2} \right) \\ \dot{\Omega}_m = \Omega_m h [-1 + \Omega_m + 2\Omega_\gamma + \Omega_\Lambda(1+3w_\Lambda)] \\ \dot{\Omega}_\gamma = \Omega_\gamma h [-2 + \Omega_m + 2\Omega_\gamma + \Omega_\Lambda(1+3w_\Lambda)] \\ \dot{\Omega}_\Lambda = \Omega_\Lambda h [-1 + \Omega_m + 2\Omega_\gamma + \Omega_\Lambda(1+3w_\Lambda) - 3w_\Lambda] \end{cases} \quad (\text{C1})$$

with boundary conditions $(h_0, \Omega_{m,0}, \Omega_{\gamma,0}, \Omega_{\Lambda,0})$. For the sake of simplicity, as in the main text, we set $\Omega_{\gamma,0} h_0^2 \approx 2.47 \times 10^{-5}$ and $\Omega_{b,0} h_0^2 \approx 0.0222$; we also consider only the case of constant equation of state $w_\Lambda = -1$ for dark energy. We then fit

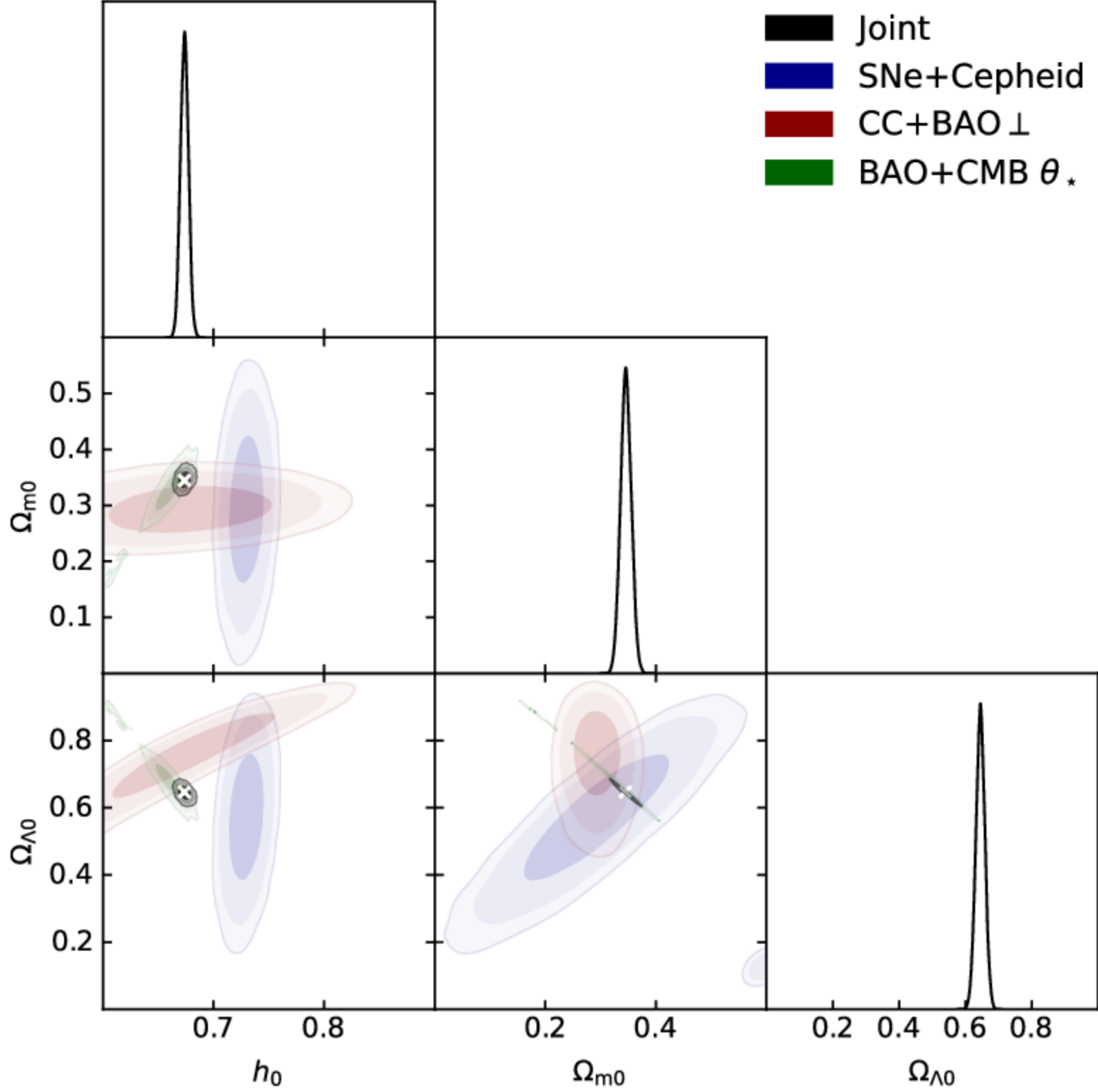


Figure C1. MCMC posterior distributions in the (curvature-free) Λ CDM model for the normalized Hubble constant h_0 , matter density parameter $\Omega_{m,0}$, and dark energy density parameter $\Omega_{\Lambda,0}$. Colored contours/lines refer to different observables: blue for SN+Cepheid, orange for CC+transverse BAOs, green for isotropic BAO+CMB first peak angular position, and black for joint. The contours show 1σ – 2σ – 3σ confidence intervals, crosses mark the maximum-likelihood estimates of the joint analysis, and the marginalized distributions of the joint analysis are reported on the diagonal panels in arbitrary units (normalized to 1 at their maximum value).

Table C1

Marginalized Posterior Estimates in Terms of Mean and 1σ Confidence Interval (and Best-fit Value) for the Fits with the (Curvature-free) Λ CDM Model to Different Cosmological Data Sets, as Listed in the First Column

| Data Set | h_0 | $\Omega_{m,0}$ | $\Omega_{\Lambda,0}$ | χ_r^2 |
|-------------------|----------------------------------|-------------------------------|-------------------------------|------------|
| Joint | $0.674^{+0.004}_{-0.004}$ [0.67] | $0.35^{+0.01}_{-0.01}$ [0.35] | $0.65^{+0.01}_{-0.01}$ [0.65] | 0.74 |
| SNe+Cepheid | $0.734^{+0.005}_{-0.015}$ [0.73] | $0.30^{+0.08}_{-0.10}$ [0.29] | $0.56^{+0.14}_{-0.11}$ [0.57] | 0.29 |
| CC+BAO $_{\perp}$ | $0.69^{+0.04}_{-0.06}$ [0.69] | $0.31^{+0.01}_{-0.05}$ [0.29] | $0.75^{+0.10}_{-0.06}$ [0.78] | 0.55 |
| BAO+CMB | $0.66^{+0.01}_{-0.01}$ [0.66] | $0.33^{+0.03}_{-0.02}$ [0.32] | $0.68^{+0.03}_{-0.04}$ [0.68] | 0.29 |








Note. Other columns report the values of the normalized Hubble constant h_0 , present matter energy density $\Omega_{m,0}$, dark energy density $\Omega_{\Lambda,0}$, and reduced χ_r^2 of the various fits.

such a model to the cosmological data sets described in Section 4 and perform a Bayesian inference on the normalized Hubble constant h_0 and the present energy density parameters of matter $\Omega_{m,0}$ and dark energy $\Omega_{\Lambda,0}$.

The marginalized constraints are shown in Figure C1 and reported in Table C1. The fits to the individual data sets produce the expected results, with SN+Cepheid mainly setting h_0 and constraining $\Omega_{m,0}$ and $\Omega_{\Lambda,0}$ with some degeneracy; the

degeneracy is removed by BAO+CMB data, which basically requires a flat Universe. From the one-dimensional posterior, the h_0 tension between late- and early-time measurements is also quite evident, with BAO+CMB data preferring lower values with respect to SN+Cepheid. The H_0 tension is at the origin of the weird behavior of the joint analysis posterior, which tends to be maximized in a region where the Universe is flat but close to the h_0 determination from CMB+BAO; clearly, the joint analysis is barely significant when the individual fits are discordant on one crucial parameter like in the Λ CDM model.

ORCID iDs

Andrea Lapi  <https://orcid.org/0000-0002-4882-1735>
 Lumen Boco  <https://orcid.org/0000-0003-3127-922X>
 Marcos M. Cueli  <https://orcid.org/0000-0003-4537-0075>
 Balakrishna S. Haridasu  <https://orcid.org/0000-0002-9153-1258>
 Tommaso Ronconi  <https://orcid.org/0000-0002-3515-6801>
 Carlo Baccigalupi  <https://orcid.org/0000-0002-8211-1630>
 Luigi Danese  <https://orcid.org/0000-0003-1186-8430>

References

- Adamek, J., Clarkson, C., Daverio, D., Durrer, R., & Kunz, M. 2018, *CQGr*, **36**, 014001
- Andrade, U., Bengaly, C. A. P., Alcaniz, J. S., & Capozziello, S. 2019, *MNRAS*, **490**, 4481
- Alam, S., Ata, M., Bailey, S., et al. 2017, *MNRAS*, **470**, 2617
- Allen, S. W., Evrard, A. E., & Mantz, A. B. 2011, *ARA&A*, **49**, 409
- Amin, M. A., & Baumann, D. 2016, *JCAP*, **2**, 45
- Amon, A., & Efstathiou, G. 2022, *MNRAS*, **516**, 5355
- Amon, A., Gruen, D., Troxel, M. A., et al. 2022, *PhRvD*, **105**, 3514
- Angulo, R. E., & Hahn, O. 2022, *LRCA*, **8**, 1
- Asgari, M., Lin, C.-A., Joachimi, B., et al. 2021, *A&A*, **645**, A104
- Ata, M., Baumgarten, F., Bautista, J., et al. 2018, *MNRAS*, **473**, 4773
- Atrio-Barandela, F., Kashlinsky, A., Ebeling, H., Fixsen, D. J., & Kocevski, D. 2015, *ApJ*, **810**, 143
- Aubourg, E., Bailey, S., & Bautista, J. E. 2015, *PhRvD*, **92**, 123516
- Aver, E., Olive, K. A., & Skillman, E. D. 2015, *JCAP*, **1507**, 011
- Avila, F., Novaes, C. P., Bernui, A., & de Carvalho, E. 2018, *JCAP*, **12**, 41
- Avila, F., Oliveira, J., Dias, M. L. S., & Bernui, A. 2023, *BriPh*, **53**, 49
- Barausse, E., Matarrese, S., & Riotto, A. 2005, *PhRvD*, **71**, 063537
- Bautista, J. E., Paviot, R., Vargas Magana, M., et al. 2021, *MNRAS*, **500**, 736
- Bengaly, C. A. P., Maartens, R., Randriamiarinarivo, N., & Baloyi, A. 2019, *JCAP*, **9**, 25
- Bennett, C. L., Halpern, M., Hinshaw, G., et al. 2003, *ApJS*, **148**, 1
- Bernal, C., Cardenas, V. H., & Motta, V. 2017, *PhLB*, **765**, 163
- Beutler, F., Blake, C., Colless, M., et al. 2011, *MNRAS*, **416**, 3017
- Bladt, M., & Sørensen, M. 2014, *Bernoulli*, **20**, 645
- Bond, J. R., Cole, S., Efstathiou, G., & Kaiser, N. 1991, *ApJ*, **379**, 440
- Borghi, N., Moresco, M., & Cimatti, A. 2022, *ApJL*, **928**, L4
- Brevik, I., Elizalde, E., Nojiri, S., & Odintsov, S. D. 2011, *PhRvD*, **84**, 3508
- Brout, D., Scolnic, D., Popovic, B., et al. 2022, *ApJ*, **938**, 110
- Bruzual, G., & Charlot, S. 2003, *MNRAS*, **344**, 1000
- Buchert, T. 2008, *GReGr*, **40**, 467
- Buchert, T., & Ehlers, J. 1997, *A&A*, **320**, 1
- Buchert, T., & Räisänen, S. 2012, *ARNPS*, **62**, 57
- Buchert, T. 2018, *MNRAS*, **473**, L46
- Celerier, M.-N. 2000, *A&A*, **353**, 63
- Chiochetta, C., Gruppuso, A., Lattanzi, M., Natoli, P., & Pagano, L. 2021, *JCAP*, **8**, 15
- Clifton, T. 2013, *IJMPD*, **22**, 1330004
- Clifton, T., Ferreira, P. G., Padilla, A., & Skordis, C. 2012, *PhR*, **513**, 1
- Coles, P., & Jones, B. 1991, *MNRAS*, **248**, 1
- Colin, J., Mohayaee, R., Rameez, M., & Sarkar, S. 2019, *A&A*, **631**, L13
- Cosmai, L., Fanizza, G., Sylos Labini, F., Pietronero, L., & Tedesco, L. 2019, *CQGr*, **36**, 5007
- Cruces, D. 2022, *Univ.*, **8**, 334
- de Mattia, A., Ruhlmann-Kleider, V., Raichoor, A., et al. 2021, *MNRAS*, **501**, 5616
- Deledicque, V. 2022, *FoPh*, **52**, 57
- Delyon, B., & Hu, Y. 2006, *Stochastic Process. Appl.*, **116**, 1660
- Di Valentino, E., Mena, O., Pan, S., et al. 2021, *CQGr*, **38**, 153001
- du Mas des Bourboux, H., Rich, J., Font-Ribera, A., et al. 2020, *ApJ*, **901**, 153
- Durham, G. B., & Gallant, A. R. 2002, *J. Bus. Econ. Stat.*, **20**, 297
- Efstathiou, G. 2020, arXiv:2007.10716
- Efstathiou, G. 2023, *A&G*, **64**, 1.21
- Efstathiou, G., & Gratton, S. 2020, *MNRAS*, **496**, L91
- Eisenstein, D. J., & Hu, W. 1998, *ApJ*, **496**, 605
- Eisenstein, D. J., Zehavi, I., Hogg, D. W., et al. 2005, *ApJ*, **633**, 560
- Ellis, G. F. R., & Stoeger, W. R. 2009, *MNRAS*, **398**, 1527
- Eyink, G. L., & Drivas, T. D. 2015, arXiv:1509.04941
- Foreman-Mackey, D., Hogg, D. W., Lang, D., & Goodman, J. 2013, *PASP*, **125**, 306
- Freese, K., & Lewis, M. 2002, *PhLB*, **540**, 1
- Friday, T., Clowes, R. G., & Williger, G. M. 2022, *MNRAS*, **511**, 4159
- Gonçalves, R. S., Carvalho, G. C., Andrade, U., et al. 2021, *JCAP*, **3**, 29
- Harikane, Y., Ouchi, M., Oguri, M., et al. 2023, *ApJS*, **265**, 5
- Hazra, D. K., & Shafieloo, A. 2015, *JCAP*, **11**, 012
- Heng, J., De Bortoli, V., Doucet, A., & Thornton, J. 2022, arXiv:2111.07243
- Herrera-Zamorano, L., Hernández-Almada, A., & García-Aspeitia, M. A. 2020, *EPJC*, **80**, 637
- Heymans, C., Grocutt, E., Heavens, A., et al. 2013, *MNRAS*, **432**, 2433
- Horvath, I., Szecei, D., Hakkila, J., et al. 2020, *MNRAS*, **498**, 2544
- Hou, J., Sanchez, A. G., Ross, A. J., et al. 2021, *MNRAS*, **500**, 1201
- Hu, J. P., Wang, Y. Y., & Wang, F. Y. 2020, *A&A*, **643**, A93
- Hu, W., & Sugiyama, N. 1996, *ApJ*, **471**, 542
- Javanmardi, B., & Kroupa, P. 2017, *A&A*, **597**, A120
- Javanmardi, B., Porciani, C., Kroupa, P., & Pflamm-Altenburg, J. 2015, *ApJ*, **810**, 47
- Jiao, K., Borghi, N., Moresco, M., & Zhang, T.-J. 2023, *ApJS*, **265**, 48
- Kaiser, N. 2017, *MNRAS*, **469**, 744
- Kashlinsky, A., Atrio-Barandela, F., & Ebeling, H. 2011, *ApJ*, **732**, 1
- Kayo, I., Taruya, A., & Suto, Y. 2001, *ApJ*, **561**, 22
- Kazin, E. A., Koda, J., Blake, C., et al. 2014, *MNRAS*, **441**, 3524
- Kloeden, P. E., & Platen, E. 1992, Numerical Solution of Stochastic Differential Equations (Berlin: Springer)
- Koksbang, S.M. 2019, *JCAP*, **2019**, 036
- Kolb, E. W. 2011, *CQGr*, **28**, 164009
- Krauss, L. M., & Chaboyer, B. 2003, *Sci*, **299**, 65
- Krishnan, C., Mohayaee, R., Colgáin, E. Ó, Sheikh-Jabbari, M. M., & Yin, L. 2022, *PRD*, **105**, 063514
- Kumar Aluri, P., Cea, P., Chingangbam, P., et al. 2023, *CQGr*, **40**, 094001
- Labbé, I., van Dokkum, P., Nelson, E., et al. 2023, *Natur*, **616**, 266
- Lapi, A., & Danese, L. 2020, *ApJ*, **903**, 117
- Lapi, A., Ronconi, T., & Danese, L. 2022, *ApJ*, **941**, 14
- Libeskind, N. I., van de Weygaert, R., Cautun, M., et al. 2018, *MNRAS*, **473**, 1195
- Lima, J. A. S., Portugal, R., & Waga, I. 1988, *PhRvD*, **37**, 2755
- Lima, J. A. S., Silva, F. E., & Santos, R. C. 2008, *CQGr*, **25**, 5006
- Lindstrom, E. 2012, *Stat. Comput.*, **22**, 615
- Lopez, A. M., Clowes, R. G., & Williger, G. M. 2022, *MNRAS*, **516**, 1557
- Macpherson, H. J., Price, D. J., & Lasky, P. D. 2019, *PhRvD*, **99**, 063522
- Magana, J., Amante, M. H., Garcia-Aspeitia, M. A., & Motta, V. 2018, *MNRAS*, **476**, 1036
- Mantinan, M., Mazzitelli, F. D., & Trombetta, L. G. 2023, *Entrp*, **25**, 151
- Mantz, A. B., Morris, R. G., Allen, S. W., et al. 2022, *MNRAS*, **510**, 131
- Maraston, C., & Stromback, G. 2011, *MNRAS*, **418**, 2785
- Marra, V., Kolb, E. W., Matarrese, S., & Riotto, A. 2007, *PhRvD*, **76**, 3004
- Martizzi, D., Vogelsberger, M., & Artale, M. C. 2019, *MNRAS*, **486**, 3766
- McConville, R., & Colgáin, E. O. 2023, arXiv:2304.02718
- Migkas, K., Pacaud, F., Schellenberger, G., et al. 2021, *A&A*, **649**, A151
- Migkas, K., Schellenberger, G., Reiprich, T. H., et al. 2020, *A&A*, **636**, A15
- Mitzenmacher, M. 2004, *Internet Math.*, **1**, 226
- Mo, H. J., & White, S. D. M. 1996, *MNRAS*, **282**, 347
- Moreno, M. V., Barci, D. G., & Gonzalez Arenas, Z. 2019, *PhRvE*, **99**, 032125
- Moresco, M. 2015, *MNRAS*, **450**, L16
- Moresco, M., Amati, L., Amendola, L., et al. 2022, *LRR*, **25**, 6
- Moresco, M., Cimatti, A., Jimenez, R., et al. 2012a, *JCAP*, **8**, 006
- Moresco, M., Verde, L., Pozzetti, L., Jimenez, R., & Cimatti, A. 2012b, *JCAP*, **7**, 53
- Moresco, M., Jimenez, R., Verde, L., et al. 2016, *JCAP*, **12**, 39
- Nakao, K.-i., Nambu, Y., & Sasaki, M. 1988, *PhThPh*, **80**, 1041
- Nelson, B., Ford, E. B., & Payne, M. J. 2014, *ApJS*, **210**, 11
- Neyrinck, M., Genel, S., & Stucker, J. 2022, arXiv:2206.10666
- Neyrinck, M. C., Szapudi, I., & Szalay, A. S. 2009, *ApJL*, **698**, L90

- Nojiri, S., Odintsov, S. D., & Oikonomou, V. K. 2017, *PhR*, 692, 1
- Paul, W., & Baschnagel, J. 2013, *Stochastic Processes from Physics to Finance* (Berlin: Springer)
- Pedersen, A. R. 1995, *Scand. J. Stat.*, 22, 55
- Perlmutter, S., Aldering, G., Goldhaber, G., et al. 1999, *ApJ*, 517, 565
- Planck Collaboration, Ade, P. A. R., Aghanim, N., et al. 2013, *A&A*, 571, A16
- Planck Collaboration, Ade, P. A. R., Aghanim, N., et al. 2016, *A&A*, 594, A14
- Planck Collaboration, Aghanim, N., Akrami, Y., et al. 2020a, *A&A*, 641, A6
- Planck Collaboration, Akrami, Y., Ashdown, M., et al. 2020b, *A&A*, 641, A7
- Racz, G., Dobos, L., Beck, R., Szapudi, I., & Csabai, I. 2017, *MNRAS*, 469, L1
- Rahman, W., Trotta, R., Boruah, S. S., Hudson, M. J., & van Dyk, D. A. 2022, *MNRAS*, 514, 139
- Raichoor, A., de Mattia, A., Ross, A. J., et al. 2021, *MNRAS*, 500, 3254
- Räsänen, S. 2010, *JCAP*, 2010, 018
- Ratsimbazafy, A. L., Loubser, S. I., Crawford, S. M., et al. 2017, *MNRAS*, 467, 3239
- Reed, W. J., & Jorgensen, M. 2004, *Commun. Stat.*, 33, 1733
- Repp, A., & Szapudi, I. 2017, *MNRAS*, 464, L21
- Repp, A., & Szapudi, I. 2018, *MNRAS*, 473, 3598
- Riess, A. G., Yuan, W., Macri, L. M., et al. 2022, *ApJL*, 934, L7
- Ripa, J., & Shafieloo, A. 2019, *MNRAS*, 486, 3027
- Risken, H. 1996, *The Fokker–Planck Equation: Methods of Solution and Applications* (Berlin: Springer)
- Rogers, G. L. C., & Williams, D. 2000, *Diffusions, Markov Processes and Martingales* (Cambridge: Cambridge Univ. Press)
- Ross, A. J., Samushia, L., Howlett, C., et al. 2015, *MNRAS*, 449, 835
- Salopek, D. S., & Bond, J. R. 1990, *PhRvD*, 42, 3936
- Saridakis, E. N., Lazkoz, R., Salzano, V., et al. 2021, arXiv:2105.12582
- Sarkar, S., Pandey, B., & Khatri, R. 2019, *MNRAS*, 483, 2453
- Schander, S., & Thiemann, T. 2021, *FrASS*, 8, 113
- Scolnic, D., Brout, D., Carr, A., et al. 2022, *ApJ*, 938, 113
- Scolnic, D. M., Jones, D. O., Rest, A., et al. 2018, *ApJ*, 859, 101
- Secco, L. F., Samuroff, S., Krause, E., et al. 2022, *PhRvD*, 105, 023515
- Secrest, N. J., von Hausegger, S., Rameez, M., et al. 2021, *ApJL*, 908, L51
- Secrest, N. J., von Hausegger, S., Rameez, M., Mohayaee, R., & Sarkar, S. 2022, *ApJL*, 937, L31
- Shandarin, S., Habib, S., & Heitmann, K. 2012, *PhRvD*, 85, 083005
- Siewert, T. M., Schmidt-Rubart, M., & Schwarz, D. J. 2021, *A&A*, 653, A9
- Simon, J., Verde, L., & Jimenez, R. 2005, *PRD*, 71, 3001
- Sivakumar, C., John, M. V., & Babu, J. K. 2001, *Prama*, 56, 477
- Springel, V., Frenk, C. S., & White, S. D. M. 2006, *Natur*, 440, 1137
- Starobinski, A. A. 1986, in *Field Theory, Quantum Gravity, and Strings*, Lecture Notes in Physics, ed. H. T. de Vega & N. Sanchez (New York: Springer), 107
- Stern, D., Jimenez, R., Verde, L., Stanford, S. A., & Kamionkowski, M. 2010, *ApJS*, 188, 280
- Tarnopolski, M. 2017, *MNRAS*, 472, 4819
- ter Braak, C. J. F., & Vrugt, J. A. 2008, *Stat. Comput.*, 18, 435
- Tiwari, P., Zhao, G.-B., & Nusser, A. 2023, *ApJ*, 943, 116
- Turner, M. S. 2022, *ARNPS*, 72, 1
- Valcin, D., Jimenez, R., Verde, L., Bernal, J. L., & Wandelt, B. D. 2021, *JCAP*, 8, 17
- Vilenkin, A. 1983, *PhRvD*, 27, 2848
- Visser, M. 2005, *GRGr*, 37, 1541
- Vogelsberger, M., Genel, S., Springel, V., et al. 2014, *MNRAS*, 444, 1518
- Watkins, R., Allen, T., Bardford, C. J., et al. 2023, *MNRAS*, 524, 1885
- Weinberg, S. 1989, *RvMP*, 61, 1
- Whitaker, G. A., Golightly, A., Boys, R. J., & Sherlock, C. 2017, *Stat. Comput.*, 27, 885
- White, S. D. M., Navarro, J. F., Evrard, A. E., & Frenk, C. S. 1993, *Natur*, 366, 429
- Wilding, G., Nevenzeel, K., & van de Weygaert, R. 2021, *MNRAS*, 507, 2968
- Wiltshire, D. L. 2007, *PhRvD*, 99, 1101
- Xiao, M., Oesch, P. A., Elbaz, D., et al. 2023, *Natur*, submitted, arXiv:2309.02492
- Xu, L. 2012, *EPJC*, 72, 2134
- Zel'dovich, Y. B. 1968, *SvPhU*, 11, 381
- Zhai, Z., & Percival, W. J. 2022, *PhRvD*, 106, 103527
- Zhang, C., Zhang, H., Yuan, S., et al. 2014, *RAA*, 14, 1221
- Zhao, C., Variu, A., He, M., et al. 2022, *MNRAS*, 511, 5492